Role of Dopants Chemistry and Particle Size on Antibacterial Efficacy of Hydroxyapatite (HAp) Powders for Bone Tissue Engineering Applications

A thesis submitted towards partial fulfillment of the requirements for the award of degree of

MASTER OF ENGINEERING

In

BIOMEDICAL ENGINEERING

Submitted by

TARANGA CHAKRAVARTY

Examination Roll No. **M4BMD22012**

Class Roll No. **002030201013**

Registration No. **154637 of 2020 - 2021**

Under the Guidance of

Dr. Subhadip Bodhak

Principal Scientist

Bio-ceramics and Coating Division

CSIR – Central Glass and Ceramic Research Institute

Kolkata - 700032

Dr. Piyali Basak

Director and Associate Professor

School of Bioscience and Engineering

Jadavpur University

Kolkata - 700032

Course affiliated to

Faculty of Engineering and Technology

Jadavpur University

Kolkata – 700032

India

2022

M.E. (Biomedical Engineering) course affiliated to

Faculty of Engineering and Technology

Jadavpur University

Kolkata – 700032

CERTIFICATE OF RECOMMENDATION

This is to certify that the thesis entitled "**Role of Dopants Chemistry and Particle Size on Antibacterial Efficacy of Hydroxyapatite (HAp) Powders for Bone Tissue Engineering Applications"** is a genuine work carried out by **TARANGA CHAKRAVARTY** under our supervision and guidance for partial fulfillment of the requirement for Post Graduate Degree of Master of Engineering in Biomedical Engineering during the academic session 2020 – 2022.

THESIS CO-ADVISOR

Dr. Subhadip Bodhak

Principal Scientist

Bio-ceramics and Coating Division

CSIR – Central Glass and Ceramic Research Institute

Kolkata - 700032

THESIS ADVISOR

Dr. Piyali Basak

Associate Professor

School of Bioscience and Engineering

Jadavpur University

Kolkata - 700032

DIRECTOR

School of Bioscience and Engineering

Jadavpur University

Kolkata - 700032

DEAN

Faculty Council of Interdisciplinary Studies, Law and Management

Jadavpur University

Kolkata - 700032

M.E. (Biomedical Engineering) course affiliated to

Faculty of Engineering and Technology

Jadavpur University

Kolkata – 700032

CERTIFICATE OF APPROVAL

This foregoing thesis is hereby approved as a creditable study of an Engineering subject carried out and presented in a manner satisfactory to warrant its acceptance as a prerequisite to the degree for which it has been submitted. It is understood that by this approval the undersigned do not necessarily endorse or approve any statement made, opinion expressed or conclusion drawn therein but approve the thesis only for the purpose for which it has been submitted.

THESIS CO-ADVISOR

Dr. Subhadip Bodhak

Principal Scientist

Bio-ceramics and Coating Division

CSIR – Central Glass and Ceramic Research Institute

Kolkata - 700032

THESIS ADVISOR

Dr. Piyali Basak

Associate Professor

School of Bioscience and Engineering

Jadavpur University

Kolkata - 700032

SIGNATURE OF EXAMINER

DECLARATION OF ORIGINALITY AND COMPLIANCE OF ACADEMIC ETHICS

I hereby declare that this thesis contains literature survey and original research work by the undersigned candidate, as part of his Master of Engineering in Biomedical Engineering studies during academic session 2020 – 2022.

All information in this document has been obtained and presented in accordance with academic rules and ethical conduct.

I also declare that, as required by this rules and conduct I have fully cited and referred all material and results that are not original to this work.

NAME: TARANGA CHAKRAVARTY

CLASS ROLL NO. 002030201013

EXAMINATION ROLL NO. M4BMD22012

REGISTRATION NO. 154637 of 2020 - 2021

THESIS TITLE: **Role of Dopants Chemistry and Particle Size on Antibacterial Efficacy of Hydroxyapatite (HAp) Powders for Bone Tissue Engineering Applications.**

_____ _____

SIGNATURE **DATE**

ACKNOWLEDGEMENT

I would like to take this opportunity to express my sincere appreciation and indebtedness to persons whose help, support and wishes have been a source of inspiration and strength during the entire thesis work.

I would like to thank Dr. Suman K. Mishra, Director, CSIR-CGCRI for giving me an opportunity to carry out this work in this prestigious institution. I would like to thank Dr. Vamsi K. Balla, Head and Chief Scientist, Bio-ceramics and Coating Division, for providing the opportunity to work in the division and for encouragement and helpful discussions regarding this work.

I would like to thank Dean, Faculty Council of Interdisciplinary Studies, Law and Management, Jadavpur University for allowing me to carry out my thesis work at CSIR-CGCRI. I would like to thank my supervisors Dr. Subhadip Bodhak, Principal Scientist, Bio-ceramics and Coating Division and Dr. Piyali Basak, Director and Associate Professor, School of Bioscience and Engineering, Jadavpur University for their support, guidance and encouragement in carrying out this thesis work. Throughout this work they shared their research experiences and knowledge which helped me to understand new concepts. They gave me freedom to work and explore various ideas related to bio-ceramic coatings and which led to the successful completion of this thesis.

I thank all the technical officers and technicians in central facility at CSIR-CGCRI who helped me in carrying out various characterizations. I would like to thank all my seniors in Bio-Ceramics and Coating Division for their friendly support and encouragement. I specially thank Moumita Debroy, Sutanu Dutta, Sankhadip Saha, Himanka Das, Anisha Kabir, Sweta Shaw, Hasanur Rahaman, Rathina Vel, Somoshree Sengupta and Anuradha Jana for their help in my thesis work.

I would also like express my gratitude to my seniors Pratik Das and Tathagata Adhikary from Biomaterials and Cell Culture Laboratory, School of Bioscience and Engineering, Jadavpur University for their immense help and support during my thesis work. I extend my special appreciation towards them because of their cooperation in estimating antibacterial properties of my samples.

Finally, I would like to thank my friends, batch-mates, B.Tech professors and my school teachers for their parts in my professional and personal life. My sincerest gratitude towards my family my father, my mother, my sister and my brother for their encouragement and moral support during my thesis work. Last but not the least, I express all my gratitude towards God for providing me with the strength to carry out this work.

Date: _____ _____

Place: Kolkata Taranga Chakravarty

Registration No.: 154637 of 2020 -2021

Roll No.: 002030201013

CONTENTS

LIST OF FIGURES

Figure 6.11 FESEM images of pure hydroxyapatite doped with zinc nanoparticles (A) at 1 weight percentage and (B) at 5 weight percentage.

Figure 6.12 FESEM images of pure hydroxyapatite doped with copper nanoparticles (A) at 1 weight percentage and (B) at 5 weight percentage.

Figure 6.13 Antibacterial efficacy of pure and different micro-sized metal oxide doped hydroxyapatite powders against *E. coli.*

Figure 6.14 Antibacterial efficacy of pure and different nano-sized metal oxide doped hydroxyapatite powders against *E. coli.*

ABSTRACT

Hydroxyapatite (HAp) based bio-ceramics hold high potential in orthopedics as synthetic bone grafts, and fillers due to their compositional similarities with native bone tissues. However, early stage infections and related inflammations are still a major challenge that often limits the wide applications of HAp based bone grafts. To address that problem, this work is focused on developing multifunctional HAp granules doped with different trace metal oxides that can offer combined benefits of improved antibacterial efficacy and enhanced osteo-conductivity. For this purpose, three different dopants (e.g., Ag, Zn and Cu) in form of metal oxide powder were incorporated into HAp at two different concentrations (1 and 5 weight percent) and *in vitro* antibacterial efficacy was assessed against growth of gram negative bacteria (i.e., *E. coli*), keeping pure HAp as a control. In this work, we have attempted to evaluate the effect of dopants chemistry as well as dopants particle size on antibacterial efficacy of pure HAp powder and identification of optimal dopants composition for potential therapeutic application as synthetic bone-graft materials. Hence, selected metal oxide powders (e.g., AgO, ZnO, and CuO) were used as dopants of HAp in both micro-sized (particle size less than 200 μm) and nano-sized (particle size less than 100 nm) form in less quantity (i.e. 1 and 5 weight percent). HAp powders were synthesized in-house by co-precipitation route and desired amount of dopants were physically mixed by ball milling and final compositions were made by sintering at 1250^{o}C. Detailed physico-chemical analyses were conducted by XRD, FTIR and FESEM prior assessing *in vitro* antibacterial efficacy. Qualitative analysis of *in vitro* antibacterial assessment was done by colony forming unit counting method. Our *in vitro* antibacterial study results demonstrated that CuO doped HAp exhibits the best antibacterial efficacy, whereas AgO and ZnO doping was found to have minimal effects amongst all groups. CuO doped HAp sample was able to inhibit bacterial growth at 100% level in 20mg/mL concentration. AgO and ZnO doped HAp samples were only able to inhibit bacterial growth by 10 – 20%. Notably nano-sized dopants incorporated HAp has higher antibacterial efficacy than that of micro-sized dopants conjugated HAp granules irrespective of dopants chemistry

Key words: Hydroxyapatite, Dopants, Metal oxide, Antibacterial efficacy, In vitro biological assays

AIM AND OBJECTIVES

Aim: Synthesis of Pure as well as micro-sized and nano-sized metal oxide powder doped hydroxyapatite powder, physico – chemical analysis of all the powder samples and their *in vitro* assessment of antibacterial properties.

Objectives:

1. Synthesis of pure hydroxyapatite (HAp) powder.

2. Doping of pure hydroxyapatite with micro-sized and nano-sized dopants – Ag, Zn & Cu – at 1wt% and 5wt% concentrations.

3. Physico-chemical characterization of the pure and doped hydroxyapatite powder.

4. Assessment of in-vitro antibacterial properties of synthesized pure and doped hydroxyapatite powder.

INTRODUCTION

Hydroxyapatite (HAp), which is one of the major calcium phosphates, is widely used in the field of biomedical engineering as HAp possesses chemical constituents similar to natural bone. HAp has a chemical formula of $Ca_{10}(PO_4)_6(OH)_2$. HAp is of great interest as a biomaterial because of its biocompatibility, bioactivity, osteo-conductivity and biodegradability. HAp has several applications in the field of bio-ceramics coating of orthopedic implants, bone fillers and also drug delivery devices. The bioactivity of HAp allows bone to grow on an implant surface when HAp is applied as a coating. The new bone formation occurs through biochemical bonding. The natural apatite available in the body resembles carbonated hydroxyapatite which possesses metallic ions such as Na^+, Mg^{2+}, Sr^{2+} F^- etc. [1]. These metal ions play a major role in the process of bone mineralization. For example, metals like manganese and zinc enhances the process of osteogenesis or the process of formation of new bones. Some other metals such as copper and cobalt help in the process of angiogenesis or process of formation new nerve tissues [2]. Hydroxyapatite used as coating has a few drawbacks such as slow tissue growth in comparison to natural bone. Also healing time can be quite long as initial stability of hydroxyapatite might take some time due to its lower osteo-conductivity compared to natural bone tissue. Extensive research is still underway to increase the osteo-conductivity of HAp, to overcome the challenges associated with molecular biochemistry, surface characteristics, mechanical stress, reaction with tissue etc. On account of these issues, it is of great interest to synthesize HAp based bio-ceramics of a new kind. Hydroxyapatite has a lattice structure which can accept metallic ions substitution. Some of the metals when get incorporated into the hydroxyapatite molecule, they enhance the mechanical as well as biological properties and bio-resorbability of HAp [3-5].

In orthopedic surgeries, infections due to bacterial attachment on the implant surface after surgery can occur which may finally lead to removal of the implant in the worst case. Several studies have been conducted to prove the antibacterial efficacy of metal ions and nanoparticles such as silver, zinc, copper etc. [6-8]. Zinc and copper are naturally present inside the human body in trace quantities which play some of the vital roles in various metabolic processes. However zinc and copper in high quantities can assert toxicity. Evidence could be found since ancient times, silver is used as medicine for wounds, burnt skin, bacterial infection etc. Silver shows very low toxicity, thermal stability and is used clinically in treatment of burnt skin, dental

implants, coating of orthopedic implant made up of stainless steel, textile, purification of water, wound dressing etc. [9, 10].

This study focuses on three main dopants – silver (Ag), zinc (Zn) and copper (Cu), in two different particle size range – micro-size and nano-size. Pure hydroxyapatite or HAp was synthesized by a precipitation method using calcium hydroxide [$Ca(OH)_2$] and phosphoric acid (H_3PO_4). Temperature was maintained at 80°C and pH level at 11. The dopants were mixed in two different concentrations – 1 weight-percent and 5 weight-percent. Planetary ball milling in ethanol medium was used for doping the pure hydroxyapatite with the dopants. After ball milling, the samples were dried at 80°C to let the ethanol evaporate. The dried sample were then crushed or ground using mortar-pastel and sieved through 150 μm mesh. After sieving, the samples were sintered at 1250°C for 2h. Sintering is done to increase the density, crystallinity and to remove the impurities of the sample. Sample pellets were made using a hydraulic press machine and the green pellets were sintered at 1250°C. The sintered samples were characterized by different physic-chemical techniques such as XRD analysis, FTIR analysis, FESEM analysis.

For the antibacterial study, spread plate technique of bacterial culture was used. *E. coli*, a gram negative bacterium was used for the study. *E. coli* is known to cause some common bacterial infections such as urinary tract infection, cholangitis, cholecystitis etc. and some clinical infections such as pneumonia and neonatal meningitis. Gram negative bacteria such as *E. coli* possess thin cell membrane, which is easily penetrated by the metal ions and nanoparticles. Three different concentrations were selected to obtain the best result. These concentrations were – 5mg/mL, 10mg/mL and 20mg/mL. Pure HAp possesses no antibacterial properties, so it was selected as the control.

LITERATURE REVIEW

Pathogenic infections and trauma can cause bone and tissue defects which has various treatment options such as repair, regeneration or replacement. Generally in these types of damaged tissue cases, the two major options are auto-graft and allograft. When tissue is transplanted from one to another place in the same individual, it is called auto-graft and when tissue is transplanted from one patient to another it is called allograft. However both these techniques have certain drawbacks. The auto-graft technique can be costly; it is limited by different anatomical issues and can cause injuries at the donor site. Allograft technique has restrictions due to limitations in finding the specific tissue for a specific individual, risks of disease transmission and issues of graft rejection by the recipient's body. There is an alternative option in the field of tissue engineering to avoid the major problems associated with auto-graft and allograft which uses biomaterials for the purpose of enhancing tissue functions to replace or regenerate the damaged tissue [11, 12].

Originally the European Society of Biomaterials defined biomaterial as a nonviable material in 1976 but later the definition was modified, which states that a biomaterial is a substance which interacts with biological systems to treat, grow or replace any tissue, organ or function. Mainly, there are three types of biomaterials which are used in the field of tissue engineering, which are natural polymers, synthetic polymers and ceramic material. These various types of biomaterials have their own advantages and limitations. The use of composite material might have an important advantage so as to control the material property. In the field of biomedical engineering, to make bone graft, implants or scaffolds, ceramic substances such as hydroxyapatite (HAp), tri-calcium phosphate (TCP), bi-calcium phosphate (BCP) etc. are generally used. Scaffolds made of ceramic material are advantageous as their mechanical strength is higher and elasticity as well as brittleness is lower. These above mentioned ceramic materials possess the approximate same chemical as well as mechanical characteristics as that of bones present in the body. That means that the ceramic materials are highly biocompatible and suitable for bone tissue engineering applications. Also in the process of increased growth and differentiation of osteoblasts, these ceramic materials play a vital role [13, 14]. Various other ceramic materials have been used for the purpose of filling bone defects and covering of implants made of metals, but the application of these materials in tissue engineering is restricted

by different factors such as their fragile nature or difficulties in shaping of the implant or mechanical load bearing issues [15, 16].

4.1 PROPERTIES OF HYDROXYAPATITE

Hydroxyapatite or HAp is a naturally available chemical constituent of bone, is biodegradable in nature and enhances osteo-integration [17]. When HAp is used as a coating material of orthopedic implants, the process of bone formation get enhanced as the HAp interacts with the natural apatite of the body enhancing bone cell growth. The different mechanical properties of synthetic HAp can be controlled according to needs by controlling the various conditions during the synthesis stage. These important parameters include concentration of the original chemicals used, the pH of the reaction solution or the sintering temperature and duration of dwelling time at that temperature. The sintering temperature is an important parameter in the synthesis process; HAp sintered at a temperature below 300°C results in lower mechanical strength but higher bio-degradability [18]. Due to the advantage of higher biodegradability, HAp is the material of choice as a coating for different metallic implants which are generally made up of stainless steel or metallic alloys. Application of HAp as a coating material gives the implant enhanced morphological characteristics of the surface and biological interactions [19]. Among all the calcium phosphate cements, HAp is the most stable one under ambient room temperature and under the pH level of 4.2 [20, 21]. The chemical formula for HAp is $Ca_{10}(PO_4)_6(OH)_2$ and it possesses a Ca:P ratio of 1.67. The crystalline lattice structure of HAp is hexagonal in majority of the cases; however in some cases it is monoclinic also. The main difference between the hexagonal and monoclinic structures is the arrangement of the hydroxyl groups (-OH). These hydroxyl groups are arranged in directions opposite to each other in the hexagonal crystalline structure. In case of the monoclinic structure, a single column consisting of the hydroxyl groups are arranged in the same direction but different columns consisting of hydroxyl groups face in the opposite direction [22]. The various crystalline structures of HAp give itself the ability to acquire numerous ions to show variability in its composition inside a bone [23, 24]. The mechanical properties of HAp generally depend on its compositional characteristics, porosity, crystallinity, size of grains etc. Due to the brittle nature of HAp, scaffolds made up it possess higher chances of cracks and if a crack appears, there is high chance that the cracks may

propagate; thus failing the purpose of the scaffold [25]. The strength of sintered HAp scaffolds increase with decreasing sizes of grain [26]. HAp possesses certain inherent biological properties which make it very useful. Among these properties some are bioactivity, bio-affinity, biocompatibility, osteo-conductivity, osteo-integration, osteo-induction and very low toxicity as HAp consists of calcium, phosphate and hydroxyl ions as base elements. When an implant is coated with HAp and placed inside the body, the surrounding body materials form an apatite layer with the implant at the site of implantation. This can also be verified from in vitro SBF study. When HAp is placed in SBF, due to the ion exchange between the SBF and HAp, formation of apatite layer can be seen [15, 27].

4.2 MODE OF ACTION OF ANTIBACTERIAL ACTIVITY OF METAL DOPANTS

4.2.1 MODE OF ACTION OF ANTIBACTERIAL ACTIVITY OF SILVER

For decades, research has been done on the antibacterial activity of silver. Silver in its ionic form as well as nanoparticle form show antibacterial properties. The concentration of silver ions is directly proportional to the antibacterial activity. With increasing concentration, antibacterial efficacy decreases on account of the oligo-dynamic effect. The various reasons behind the antibacterial properties of silver can be identified as – reaction with the surrounding outer and inner membranes of the bacterial cells, reaction with intracellular molecules such as enzymes, nucleic acids and Reactive Oxygen Species (ROS) production [28]. In both gram positive as well as gram negative bacterial it can be seen that when silver ions get accumulated in the outer cell membrane or cell wall, it starts to separate the cytoplasmic membrane away from the cell wall [29, 30]. It has also been observed that, to denature the outer cell membrane of gram positive bacteria 32 times more silver ions are needed in comparison to gram negative bacteria, as gram positive bacteria possesses a thicker cell wall [28]. However studies have reported that silver ions do not actually kill the bacteria, rather keep the bacteria in a non-active state [29]. The major difference between how silver ions kill gram positive and gram negative bacteria is the mode of entry of the ions into the cells. In case of gram negative bacteria, silver ions enter the cells with the help of outer membrane proteins [30]. Proteins such as cytochrome b which are associated with the respiratory chain system of the bacteria undergo inhibition which increases

the reactive oxygen species inside the cells. The increase in ROS leads to oxidative stress increase, protein denaturation, DNA denaturation and finally senescence. In case of protein denaturation, the silver ions bind to the bacterial ribosome and ribosomal proteins, which damage the actual structure and function of the ribosome, finally leading to the inability to synthesize proteins [31]. In case of DNA denaturation, the silver ions bind with the pyrimidine bases of the DNA strand which leads to DNA condensation and finally inhibition of replication [32]. The actual mechanism of action of silver nanoparticles is still under research, it is evident that the silver nanoparticles react with the cell envelop, intracellular molecules and pathways [33].

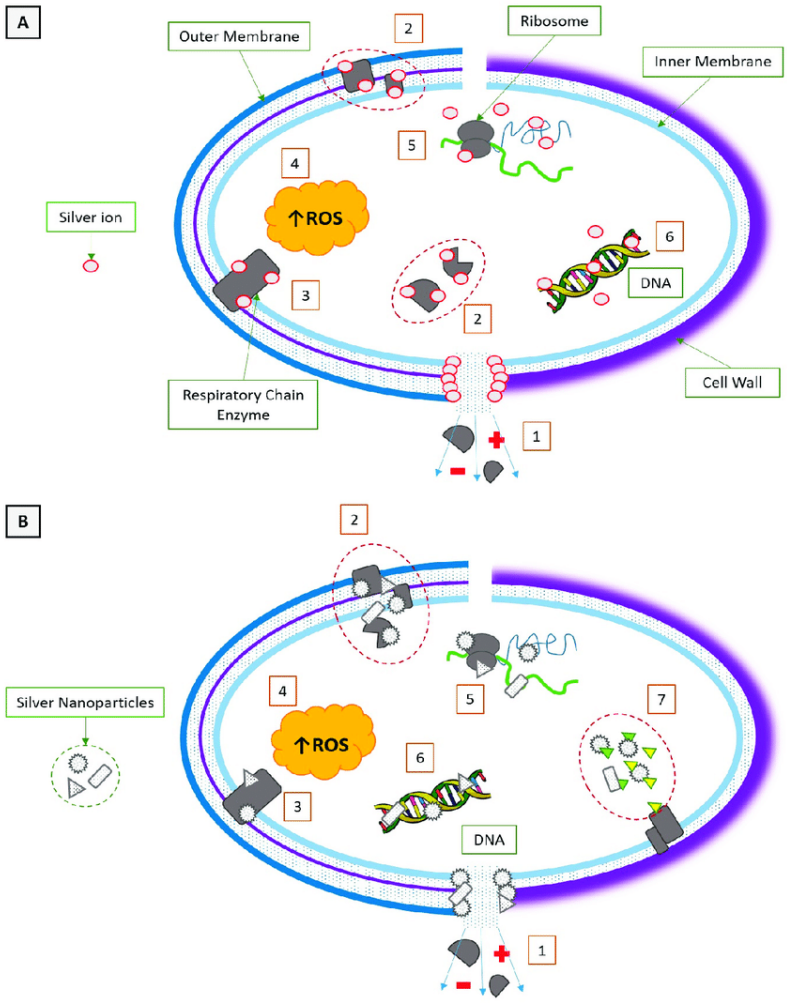

Figure 4.1 Schematic representation of mode of action of (A) silver ions and (B) silver nanoparticles. The left side depicts gram negative bacteria and the right side depicts the gram positive bacteria [34].

In brief, Figure 4.1 shows (1) formation of pores and metabolites; leakage of ions (2) rupturing of structural and cytoplasmic proteins, inactivation of enzymes (3) Proteins or enzymes associated with respiratory system inactivation (4) higher concentration of ROS inside the cell (5) different reactions with bacterial ribosome (6) reactions with nucleic acids (7) restricting intracellular signal transduction. These are the various modes or ways by which silver ions and nanoparticles show antibacterial efficacy.

4.2.2 MODE OF ACTION OF ANTIBACTERIAL ACTIVITY OF ZINC

Zinc ions play important roles in the bacterial metabolism to regulate cell proliferation as well as differentiation and to maintain the regular functional structure of the cell [35]. Along with these, zinc ions also take part in various metabolic pathways to degrade or assimilate the carbohydrate, lipid and polysaccharide molecules [36]. These functions regulate smoothly when zinc ions are in limited or less concentration. When the cell takes up a large quantity of zinc ions, it restricts the normal functioning or growth of the bacterial cells. When the cell takes up too much of Zn^{2+} ions, these ions start replacing other metal ions in various metal-binding proteins. This phenomenon finally leads to protein degeneration or enzymatic malfunction which is fatal for the bacterial cells [37, 38]. In case of zinc in its nanoparticle form, the released Zn^{2+} ions are the reason behind its antibacterial properties [39]. However, the actual mechanism behind the antibacterial properties of zinc nanoparticles is still not fully known. It has also been proposed that zinc nanoparticles are directly associated with cell wall disruption and thus killing the bacteria [40]. Zinc nanoparticles also increase the oxidative stress inside the bacterial cell by producing excess ROS, which finally kills the bacteria [41]. In case of the antibacterial efficacy of zinc, sometimes it is seen that gram positive bacteria is more susceptible compared to gram negative bacteria [42]. It can be interpreted that in case zinc nanoparticles the antibacterial properties depend on sensitivity of a particular organism. Due to the positive charge of the zinc ions and negative charge of the cell membrane, a strong ionic bond is formed between the two because of electrostatic attraction. When Zn^{2+} ions bind to the cell membrane, it increases the permeability of the cell membrane as a result zinc nanoparticles enter the cell in large quantity and disturbs various cellular activities. When the zinc nanoparticles directly react with the cell membrane, it disrupts the integrity of the membrane which might make the important molecules

to flow out of the cell cytoplasm. This phenomenon can be deadly for the cell [43]. Just like silver ions, upon interaction with zinc ions, the oxidative stress increases due to ROS production. When UV light or visible light of higher energy is incident on zinc oxide molecules, it undergoes reaction process due to which hydrogen peroxide and other radical molecules are produced. These radicals are strong oxidizing agents and molecules like hydrogen peroxide easily penetrates the cell membrane which increases the oxidative stress and damage the cell by disruption of proteins, DNA and peroxidation of lipid [44, 45]. However in case of some of the specific bacteria, instead of hydrogen peroxide production, it affects on anaerobic carbohydrate cycle resulting inhibition of growth. In these cases, zinc nanoparticles play a biomimetic role to carry out its action [46].

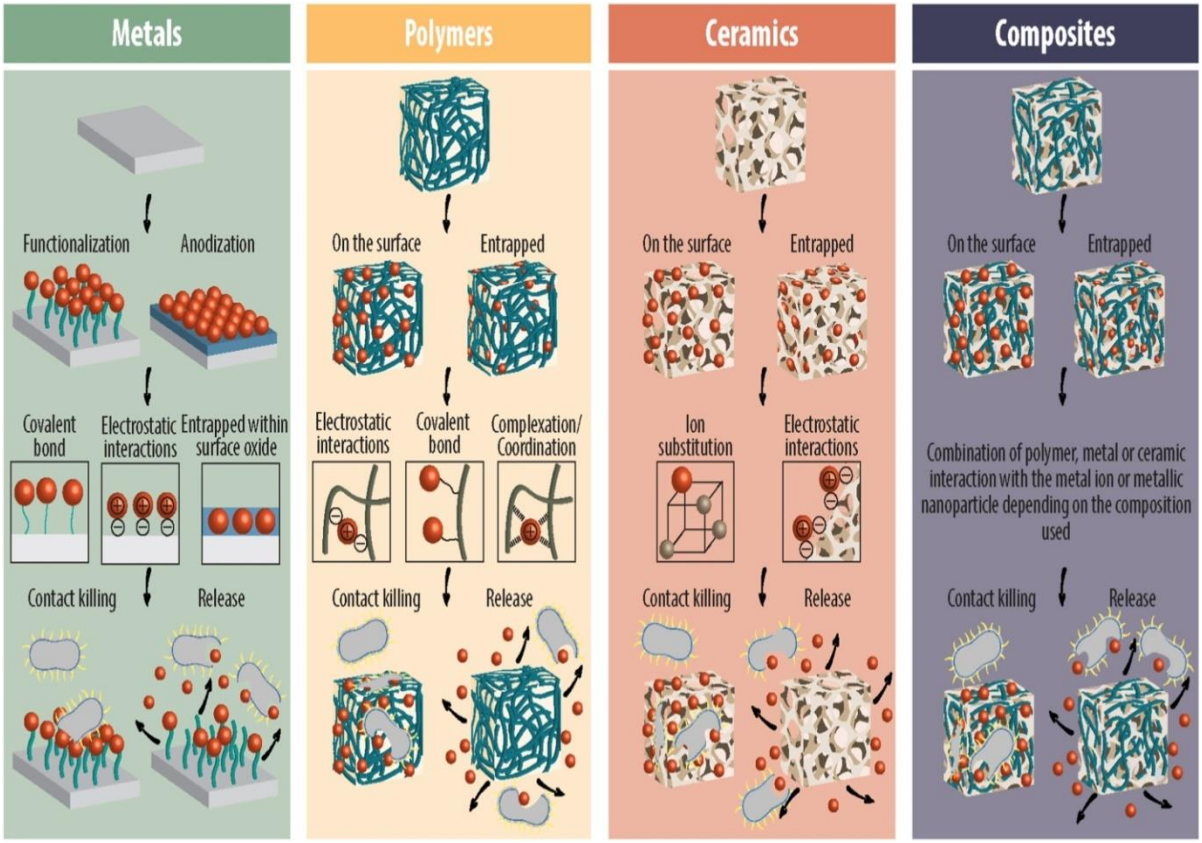

Figure 4.2 Schematic diagram showing various biomaterials conjugated with metals in their ionic or nanoparticle form. The red dots indicate ionic or nanoparticle of metals. A metal or polymer or ceramics or composite surface can be modified to hold metal ions or nanoparticles in place with the help of covalent or electrostatic interactions. The conjugated metal ions or nanoparticles impart the antibacterial properties within the material [47].

4.2.3 MODE OF ACTION OF ANTIBACTERIAL ACTIVITY OF COPPER

Copper plays a vital role as a cofactor for various important enzymes associated with respiration as well as photosynthesis system. The activity or role of copper in the metabolic processes generally depends upon its oxidation state. With respect to the oxidation state of copper, copper carries out various activities by reacting with different proteins. For example, Cu^{+} ion is attracted towards cysteine, methionine which consist thiols and thioesters, whereas Cu^{2+} ion has affinity for aspartate, glutamate, histidine etc. which have oxygen and nitrogen coordination groups [48, 49]. The actual mechanism behind the antibacterial activity of copper ions and nanoparticles is not entirely known. However, some of the factors responsible for its antibacterial activity are bacterial outer cell membrane damage, changes or irregularities in various metabolic processes, DNA disruptions etc. [50, 51]. When bacterial cell takes up copper nanoparticles, these nanoparticles react with various proteins inside as well as biomolecules and compounds which have sulfur in their structure. The copper nanoparticles release copper ions which can directly pass through the bacterial cell membrane. These ions in an excessive quantity disrupt numerous biochemical processes inside the cell and also cause DNA damage [52]. Among many hypotheses, one mentions that when copper comes in contact with bacterial cell membrane, it reacts with the phospholipids to make alterations in the cell membrane structure. These alterations change the permeability and flexibility of the membrane. This change can trigger an increase in the oxidative stress, because of accumulation of radicals on the cell membrane, which finally creates irregularities in the electron transport chain [53]. In case of gram positive bacteria, on their outer membrane they possess huge quantities of amines and carboxyl groups, which have strong affinity towards copper ions as well as copper containing compounds [52, 54]. Along with production of reactive oxygen species to increase the oxidative stress, copper ions also target the intracellular proteins to assert their antibacterial properties [55]. Proteins are generally comprised of nitrogen, oxygen and sulfur based donor groups and copper ions have a strong affinity for these types of groups. As these types of groups are present in high quantity and copper is highly reactive to them, increase in concentration of copper leads to failure of protein functions because copper causes displacement of metal ions [56-58]. Apart from increase in oxidative stress, copper also cause mismatch of metals in aerobic nucleotide synthesis mechanism. This causes irregularities in the cellular metabolism. Though the cell tries to bring back the synthesis process to normal, due to further metal mismatch in other cellular pathways, it

is not possible [56]. Also, copper breaks apart clusters of metals such as clusters of iron and sulfur. Iron-sulfur clusters can be found in different major enzymes associated with several metabolic pathways such as DNA replication, DNA damage repair, energy production mechanism etc. [59, 60]. Very little information has been acquired regarding intracellular DNA and copper interaction. Copper can bind to some of the copper sensing transcription repressing proteins [61]. Copper nanoparticles especially can bind to the double helix of DNA to disassemble the strands, which cause anomalies in the central dogma process and finally leading to cell death [62].

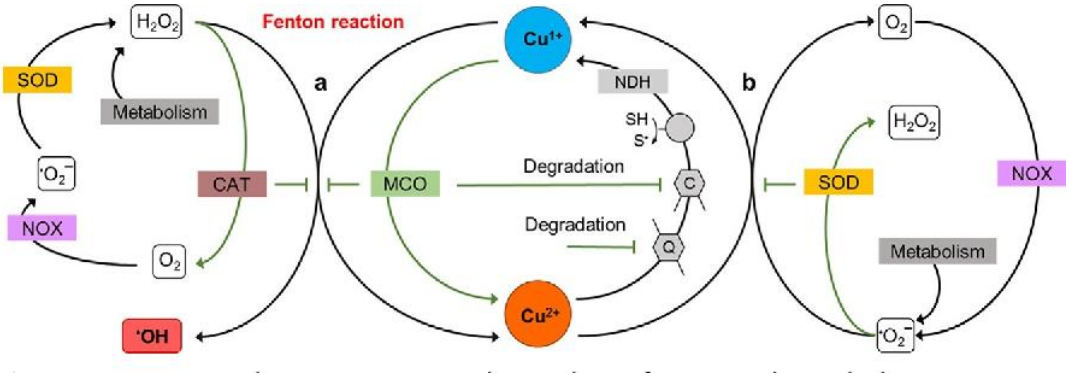

Figure 4.3 Schematic diagram of enzymatic and non-enzymatic redox cycle of copper [63].

In reaction (a), hydrogen peroxide is converted to hydroxyl radicals where copper (Cu^{1+}) acts as an inorganic catalyst. Excess production of hydroxyl radicals is harmful for the cells that is why the cells either convert Cu^{1+} to Cu^{2+} with the help of multi-copper oxidases (MCO) or decrease the levels of hydrogen peroxide by catalases (CAT). Hydrogen peroxide is produced as a metabolic byproduct arising from superoxide radicals ($\cdot O_2^-$) with the help of superoxide dismutases (SOD). $\cdot O_2^-$ is produced from oxygen (O_2) by NADPH oxidase or NOX. $\cdot O_2^-$ is one of the major reducing agents of Cu^{2+} as it can be seen in reaction (b). Copper ions undergo a continuous redox cycle when hydrogen peroxide, superoxide radicals are present and hydroxyl radicals are produced in the process. Molecules like SOD can inhibit this redox cycle by prevention of the activity of superoxide radicals. Some other examples of such molecules are quinones (Q), catechols (C), thiols (SH), NADH dehydrogenase (NDH) etc. which inhibit the redox cycle by reducing Cu^{2+}. The reduction can take place as catechol siderophores get oxidized by MCO or quinone degradation pathway gets activated. The green arrows which can be seen in the reactions represent inhibition pathways which restrict radical formation [63].

METHODOLOGY

5.1 MATERIALS USED

Calcium hydroxide, $Ca(OH)_2$ was procured from SRL Chemicals private limited [Catalogue No. 85610]. Phosphoric acid, H_3PO_4 was procured from Merck Life Science Private Limited [EMPLURA Ortho-Phosphoric acid 85%, Catalogue No. CL0C700631]. Micro particle sized Silver Oxide, AgO [Catalogue No. 221163] and Zinc Oxide, ZnO [Catalogue No. 96479] were bought from Sigma-Aldrich. Micro particle sized Cupric Oxide, CuO was bought from Loba Chemie private limited [Catalogue No. 03076]. Silver nanoparticles having particle size of less than 90 nanometers was procured from SRL Chemicals private limited [Catalogue No. 44416]. Zinc oxide, ZnO and Copper Oxide, CuO nanoparticles were bought from Sigma Aldrich [Catalogue No. 544906 and 544868 respectively]. Zinc oxide nanoparticles have particle size less than 100 nanometers and copper oxide nanoparticles have particle size less than 50 nanometers. Nutrient Broth [Catalogue No. M002] and Agar Powder [Catalogue No. GRM026] were procured from HIMEDIA. Antibiotic Streptomycin Sulphate (STM) was bought from SRL Chemicals private limited [Catalogue No. 91014].

5.2 SYNTHESIS OF PURE HYDROXYAPATITE

Calcium hydroxide was weighed (155g) and added to 3L of distilled water. The beaker with the solution was kept on a hot plate and the powder was allowed to mix with the help of magnetic stirrer. In another beaker, 2L of distilled water was taken and 76mL of phosphoric acid was added. A burette was set over the beaker on the hot plate. The solution containing phosphoric acid was poured into the burette. When the solution containing calcium hydroxide reached 80°C of temperature, the solution of phosphoric acid was allowed to mix drop-wise. The poring rate of the phosphoric acid solution was set so that the whole 2L of solution got mixed within 90 to 120 minutes. The temperature was kept steady at 80°C and pH was maintained at 11 to 12. After both the solutions got mixed, the resultant solution containing calcium hydroxide and phosphoric acid was allowed to stir for another 30 minutes at 80°C. Finally, the solution was kept for 48h undisturbed. Once the time period of 48h was completed, the solution was filtered using a suction pump and Buchner funnel. A filtrating cloth was kept on the funnel to obtain the

hydroxyapatite powder. The obtained HAp powder was collected using a spatula and dried in a hot air oven at 80°C for 24h. After drying, the powder was ground in a mortar pastel. The ground powder was passed through a 150µm mesh to obtain fine particles. The resultant powder was then sintered at 1250°C for 2h inside a high-temperature furnace. The temperature was allowed to rise at a rate of 5°C per minute. The sintered powder was again ground in a mortar pastel and passed through a mesh of 120µm range. The final powder obtained was stored and marked as pure hydroxyapatite.

5.3 SYNTHESIS OF DOPED HYDROXYAPATITE (Ag, Zn and Cu)

Calcium hydroxide was weighed (155g) and added to 3L of distilled water. The beaker with the solution was kept on a hot plate and the powder was allowed to mix with the help of magnetic stirrer. In another beaker, 2L of distilled water was taken and 76mL of phosphoric acid was added. A burette was set over the beaker on the hot plate. The solution containing phosphoric acid was poured into the burette. When the solution containing calcium hydroxide reached 80°C of temperature, the solution of phosphoric acid was allowed to mix drop-wise. The poring rate of the phosphoric acid solution was set so that the whole 2L of solution got mixed within 90 to 120 minutes. The temperature was kept steady at 80°C and pH was maintained at 11 to 12. After both the solutions got mixed, the resultant solution containing calcium hydroxide and phosphoric acid was allowed to stir for another 30 minutes at 80°C. Finally, the solution was kept for 48h undisturbed. Once the time period of 48h was completed, the solution was filtered using a suction pump and Buchner funnel. A filtrating cloth was kept on the funnel to obtain the hydroxyapatite powder. The obtained HAp powder was collected using a spatula and dried in a hot air oven at 80°C for 24h. After drying, the powder was ground in a mortar pastel. The ground powder was passed through a 150µm mesh to obtain fine particles. All the dopants (Ag, Zn & Cu in micro and nanoparticle size) were weighed 0.3g and 1.5g each and mixed with 29.7g and 28.5g pure HAp powder respectively in specific pots used in planetary ball milling machine. In each pot, 150mL of ethanol was added and zirconia balls were added weighing 70g. The mixtures were allowed to mix in planetary ball milling machine for 72h at 200rpm. After 72h, the resultant mixture in ethanol medium was dried in a hot air over at 80°C for 24h. Then obtained dried powders were ground in a mortar pastel and passed through a mesh of 150µm

range. The ground powders were sintered at 1250°C for 2h inside a high-temperature furnace. The temperature was allowed to rise at a rate of 5°C per minute. The sintered powders were then ground in a mortar pastel and passed through a mesh of 120µm range. The obtained powders were stored and marked according to their dopant name and its weight-percentage.

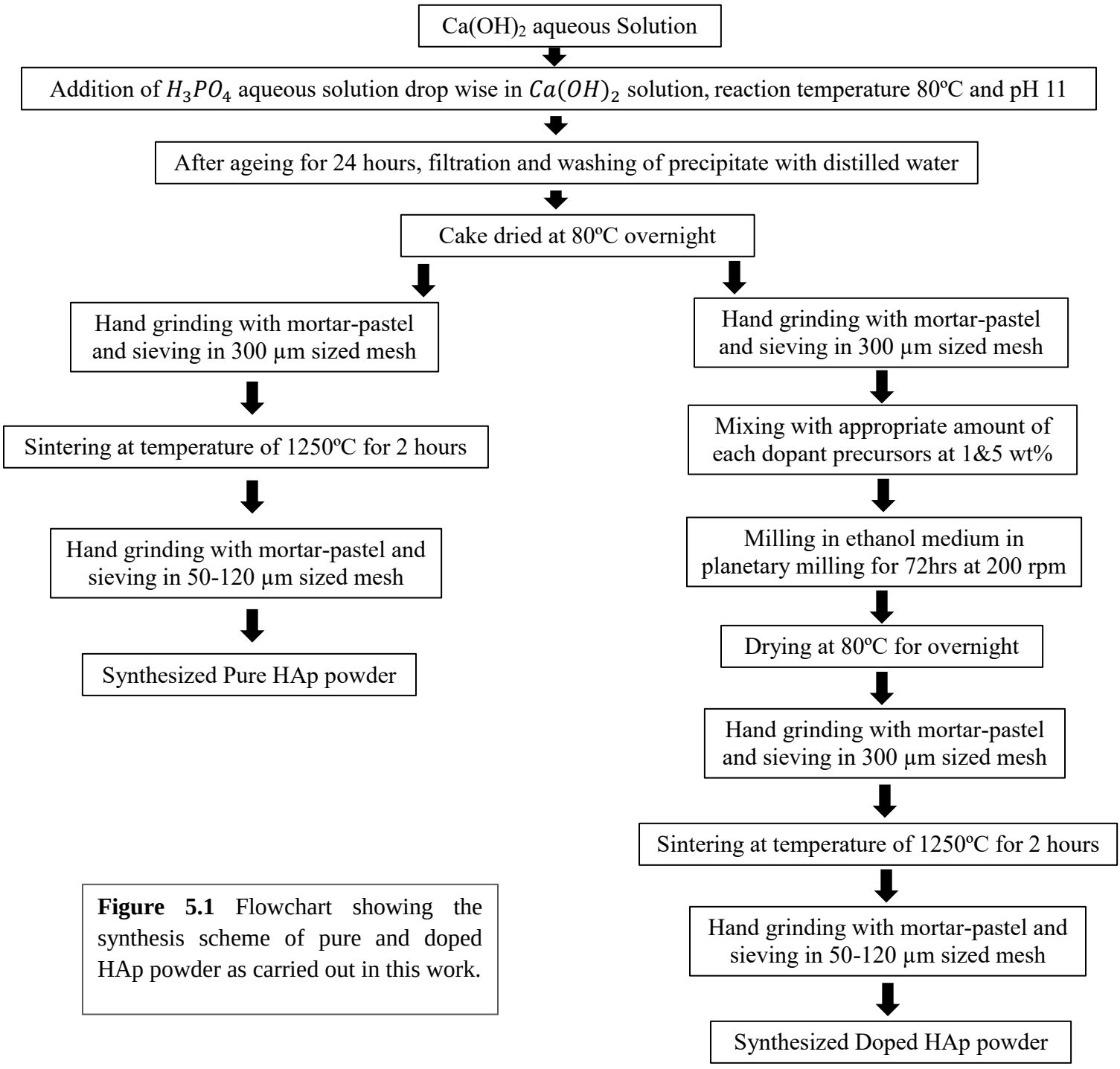

Figure 5.1 Flowchart showing the synthesis scheme of pure and doped HAp powder as carried out in this work.

5.4 PHYSICO – CHEMICAL CHARACTERIZATIONS OF SYNTHESIZED PURE AND DOPED HYDROXYAPATITE

5.4.1 PHASE ANALYSIS BY X-RAY DIFFRACTION ANALYSIS (XRD)

X-Ray Diffraction analysis machine follows the Bragg's equation which states that,

$$n\lambda = 2d\sin\Theta$$

Here, n is the order of diffraction (n = 1, 2, 3,…), λ is the wavelength of the X-rays in the machine (for generally used CuKα, λ=1.5418Å), d represents the inter-planar spacing and Θ is the Bragg angle. Scattered x-rays are incident on the material and constructive interference can be detected among these scattered rays upon the fulfillment of Bragg's law. The detector captures diffracted x-rays with respect to their different incident angles. The diffraction of the incident rays depend on the atomic arrangement of the material. Therefore XRD analysis is useful to identify the crystalline phases of a specific sample.

In this work, the synthesized pure as well as doped hydroxyapatite powders were characterized using a X-ray diffractometer (Ultima IV, Rigaku) which uses Ni – filtered CuKα radiation of wavelength 1.5418Å. The selected range was between 0° - 90°C along with a step size of 0.02 and scan rate of 6 steps per second.

Figure 5.2 X-ray diffractometer (Ultima IV, Rigaku)

5.4.2 ELEMENTAL COMPOSITION ANALYSIS BY FOURIER TRANSFORM INFRARED (FTIR) SPECTROSCOPY

Fourier transform infrared spectroscopy shows the infrared spectrum of transmission, absorption or reflection of the sample material. In this technique infrared radiation is used which passes through the sample and gets either transmitted, absorbed or reflected. When the energy of molecular vibration of the sample material matches with the incident infrared radiation energy, absorption takes place. Due to this reason, different molecular vibrations can be identified using the FTIR spectroscopy technique. FTIR spectrophotometer generally consists of an infrared radiation source, a splitter to split the incident beam, a fixed and another movable beam which are placed at right angle to one another. The beam splitter splits the incident beam into two and each beam is directed towards the fixed as well as movable mirrors. Due to the movement of the mirrors, the path difference generated between the two incident rays creates interference. When the incident rays fall on the sample material, an interferogram is obtained. By utilizing Fourier transform principle on the interferogram, the final spectrum is obtained as a function of frequency or wave number. In the final spectrum, bands can be seen which represent different molecular vibration in the sample material.

In this study, all the samples were analyzed by FTIR spectroscopy using FTIR spectrophotometer (Spectrum 100 FT-IR Spectrophotometer, Perkin Elmer). The samples were first mixed with potassium bromide (KBr) in a ratio of 1:100 and then pellets were made. The final spectrum was measured in the mid infrared region, 400 – 4000 cm^{-1}.

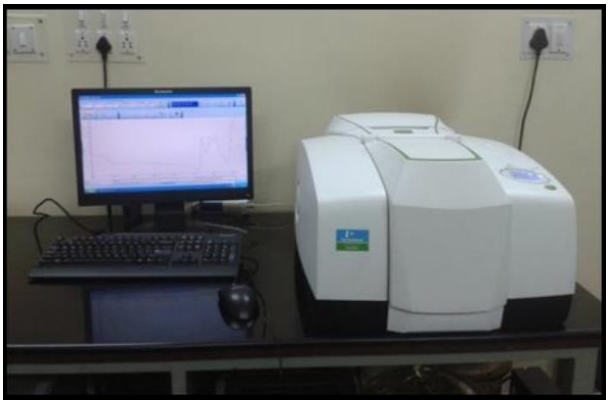

Figure 5.3 FTIR spectrophotometer (Spectrum 100 FT-IR Spectrophotometer, Perkin Elmer)

5.4.3 SURFACE MICROSTRUCTURE ANALYSIS BY FIELD EMISSION SCANNING ELECTRON MICROSCOPY (FESEM)

Field emission scanning electron microscope is used to scan the surface of a sample by a focused electron microscope. For surface microstructure and chemical composition analysis, the detector present detects the secondary electrons, backscattered electrons and characteristic x-rays which are generated when electrons hit the sample surface. Low energy electrons are called secondary electrons. Detection of secondary electrons generates an image of the sample surface. The detected backscattered electrons generate the surface topography by sensing heavy and light weight elements present. Detection of characteristic x-rays is important to obtain information about elemental composition of the surface.

In this study, field emission scanning electron microscopy (Carl Zeiss FESEM Supra 35 VP, Oberkochen, Germany) was used to analyze the surface morphology and elemental composition of all the HAp samples with dopants in nanoparticle size range. Before analyzing, all the samples were coated with carbon.

Figure 5.4 Field Emission Scanning Electron Microscope (Carl Zeiss FESEM Supra 35 VP, Oberkochen, Germany)

5.5 IN VITRO ANTIBACTERIAL ASSESSMENT

Spread plate technique of bacterial culture was used to test the antibacterial efficacy of all the samples against *E. coli*, a gram negative bacterium. This whole experiment was carried out under sterile conditions inside a laminar hood in presence of a burning lamp.

The four-day continuous experiment started with extracting a single bacterial colony with the help of a sterile culture loop from bacterial stock culture and then inoculating the colony into 5mL of liquid nutrient broth media taken in a test tube. This test tube was kept in the incubator at 37°C for 24h. On the next day, the pure and doped hydroxyapatite powder was weighed according to the pre-determined concentration – 5mg/mL, 10mg/mL and 20mg/mL. Test tubes were cleaned, nutrient broth was prepared according to the needed quantity (1.3g of nutrient broth in 100mL of distilled water) and the top of the test tubes were firmly plugged with cotton. Autoclaving was done at 121°C temperature and 15psi pressure for 15 minutes. After autoclaving, the media was allowed to cool down and the powder samples were added to each test tube. The initial bacterial culture was taken out of the incubator and pipetted into each sample test tube at a concentration of 10µL/mL. All the test tubes were marked according to their dopants and concentration and kept inside the incubator for 24h at 37°C temperature. On the third day, 2.5% nutrient agar plates were prepared. Nutrient broth, agar powder (2.5%) and distilled water were added to a conical flask and the top of the flask was plugged firmly with cotton. The nutrient agar solution was then autoclaved and transferred to the laminar hood along with sterile petri-plates. UV radiation treatment was done inside the laminar hood for 15 minutes. The nutrient agar media was allowed to cool down to 60-80°C. After that, the media was carefully poured into petri-plates without the formation of any bubbles. The plates were left undisturbed for 20 minutes. Once the agar plates had solidified, the test tubes were taken out of the incubator and placed inside the hood. The nutrient broth media in the test tubes were diluted at a concentration of 1µL in 1mL of sterile saline water. From each of the diluted solutions, 50µL was pipetted over the respective agar plates. With the help of a sterile L-shaped glass rod, the diluted bacterial solutions were homogenously spread over the agar plates. The plates were carefully kept inside the incubator at 37°C for 24h. On the next day, the plates were observed to obtain a qualitative analysis of antibacterial efficacy of different doped HAp powders at different concentrations.

RESULTS AND DISCUSSION

6.1 PHASE ANALYSIS BY X-RAY DIFFRACTION ANALYSIS OF PURE AND METAL OXIDE DOPED HYDROXYAPATITE POWDERS

6.1.1 XRD ANALYSIS OF PURE HYDROXYAPATITE

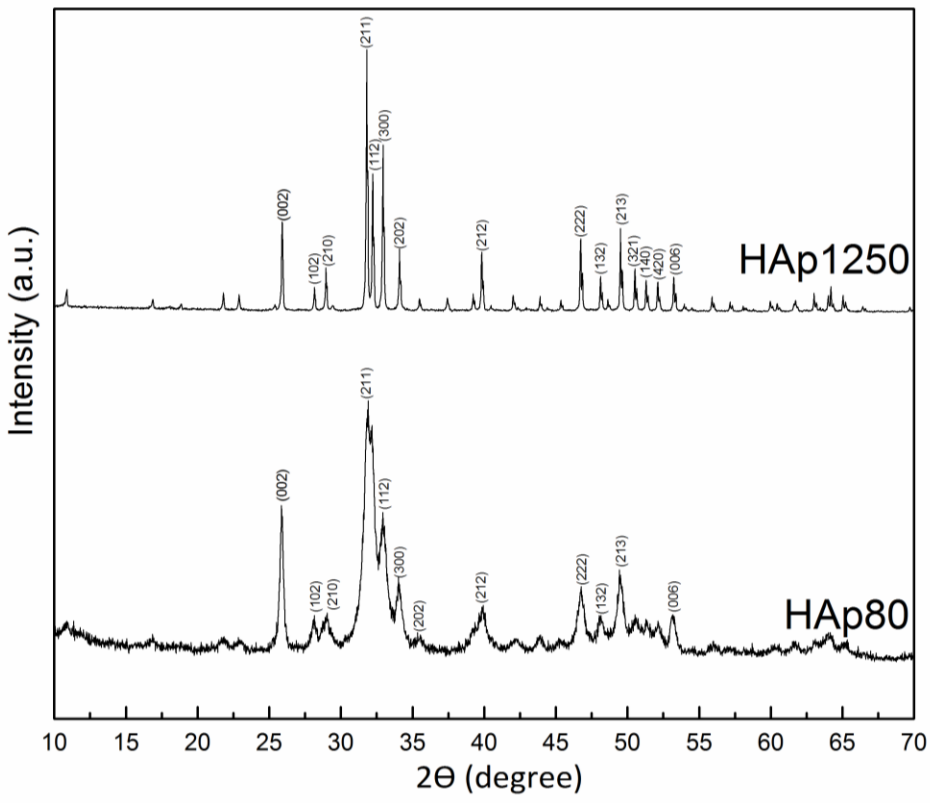

Figure 6.1 XRD Analysis of pure hydroxyapatite powder dried at 80°C and sintered at 1250°C.

X- ray diffraction analysis was done for hydroxyapatite powder dried at 80°C overnight inside a hot-air oven and for hydroxyapatite powder sintered at 1250°C for 2h inside a high temperature furnace. All the diffraction patterns were analyzed and indexed with the help of JCPDS no. 09-0432 for identification of hydroxyapatite phases. All the characteristics peaks can be seen in hydroxyapatite sintered at 1250°C. These peaks can be identified as – (002), (102), (210), (211), (112), (300), (202), (212), (222), (132), (213), (321), (140), (420) and (006). No additional peaks indicating the formation of bi-calcium phosphate (BCP) or tri-calcium phosphate (TCP) can be seen. In case of hydroxyapatite dried at the temperature of 80°C, the same peaks can be

identified. It is clearly visible from the diffraction patterns that heat treatment at the temperature of 1250°C increases the crystallinity and stability of the hydroxyapatite powder.

6.1.2 XRD ANALYSIS OF SILVER DOPED HYDROXYAPATITE

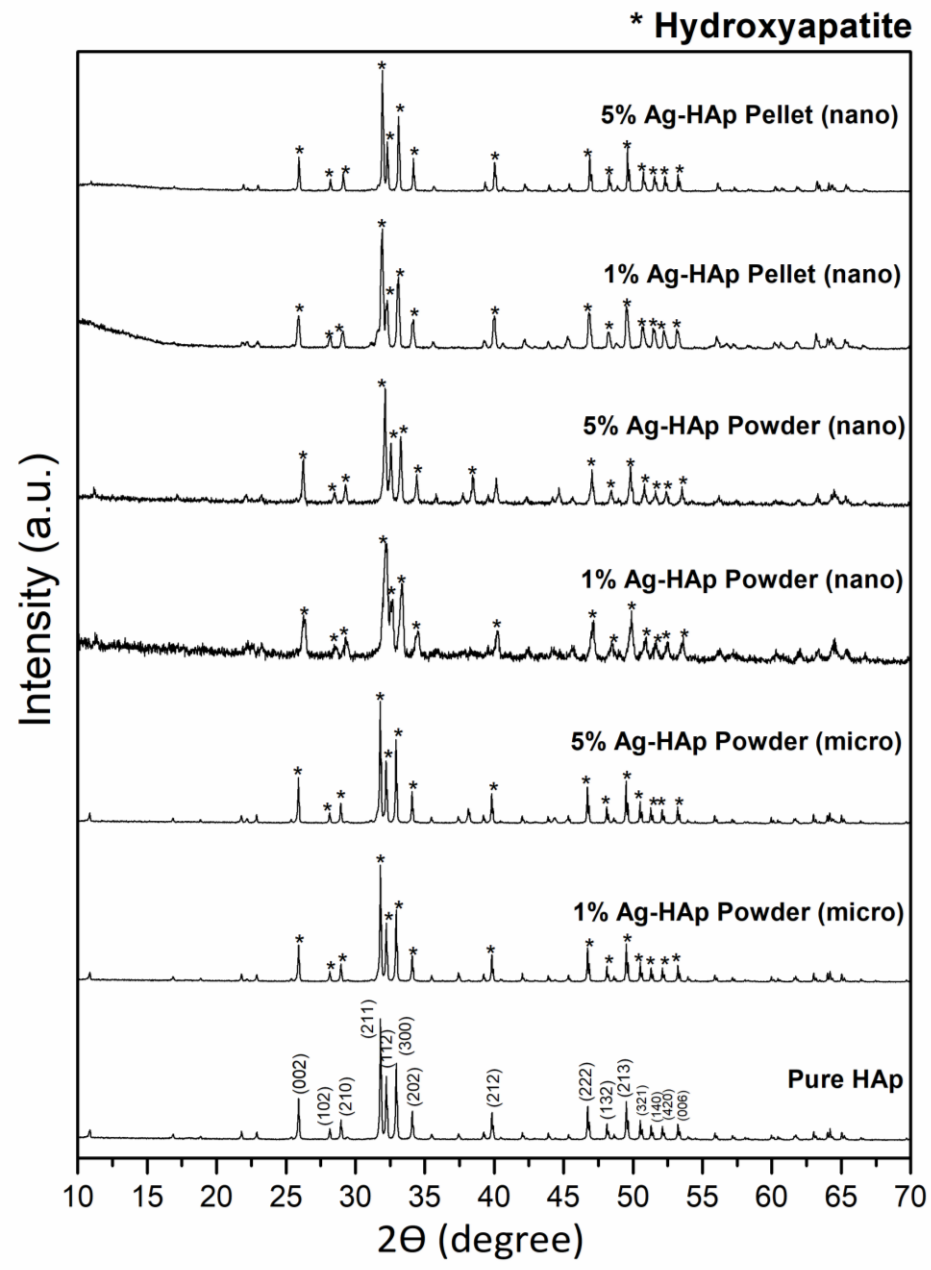

Figure 6.2 XRD analysis of hydroxyapatite powder doped with silver with respect to different concentrations and particle sizes.

Figure 6.2 contains diffraction patterns of – pure HAp powder, HAp powder doped with 1 weight percentage of silver of micro-particle size range, HAp powder doped with 5 weight percentage of silver of micro-particle size range, HAp powder doped with 1 weight percentage of silver of nanoparticle range, HAp powder doped with 5 weight percentage of silver of nanoparticle range, HAp pellet doped with 1 weight percentage of silver of nanoparticle range and HAp pellet doped with 5 weight percentage of silver of nanoparticle range. In figure 6.2, all the characteristics peaks of hydroxyapatite sintered at 1250°C can be identified as (002), (102), (210), (211), (112), (300), (202), (212), (222), (132), (213), (321), (140), (420) and (006). No major peak of any other substance such as bi-calcium phosphate (BCP), tri-calcium phosphate (TCP), tetra-calcium phosphate (TTCP) or calcium oxide can be seen in the patterns. Also pure HAp as well as all the doped samples shows a very good crystallinity and stability. In the process of wet ball milling, when the pure HAp powder and silver was added, it was expected that the resulting mixture will be homogenous. It is expected that the silver ions or nanoparticles substitute the calcium in the lattice structures. From the patterns, in HAp powders containing silver at 5 weight percentages, silver can be identified as a peak at $2\Theta = 38°$. In case of HAp powders doped with silver at 1 weight percentages, a tiny peak corresponding to silver can be seen at $2\Theta = 38°$. However the patterns of HAp pellets containing silver at 1 and 5 weight percentages of nanoparticle range, this peak indicating the presence of silver is missing. In case of all the powders doped with 5 weight percentages of silver, another small peak can be seen at around $2\Theta = 44°$, which can be another indication towards the presence of silver.

6.1.3 XRD ANALYSIS OF ZINC DOPED HYDROXYAPATITE

Figure 6.3 contains diffraction patterns of – pure HAp powder, HAp powder doped with 1 weight percentage of zinc of micro-particle size range, HAp powder doped with 5 weight percentage of zinc of micro-particle size range, HAp powder doped with 1 weight percentage of zinc of nanoparticle range, HAp powder doped with 5 weight percentage of zinc of nanoparticle range, HAp pellet doped with 1 weight percentage of zinc of nanoparticle range and HAp pellet doped with 5 weight percentage of zinc of nanoparticle range. In figure 6.3, all the characteristics peaks of hydroxyapatite sintered at 1250°C can be identified as (002), (102), (210), (211), (112), (300), (202), (212), (222), (132), (213), (321), (140), (420) and (006). No major peak of any

other substance such as bi-calcium phosphate (BCP), tri-calcium phosphate (TCP), tetra-calcium phosphate (TTCP) or calcium oxide can be seen in the patterns. Also pure HAp as well as all the doped samples shows good apatite phases and very good crystallinity, stability.

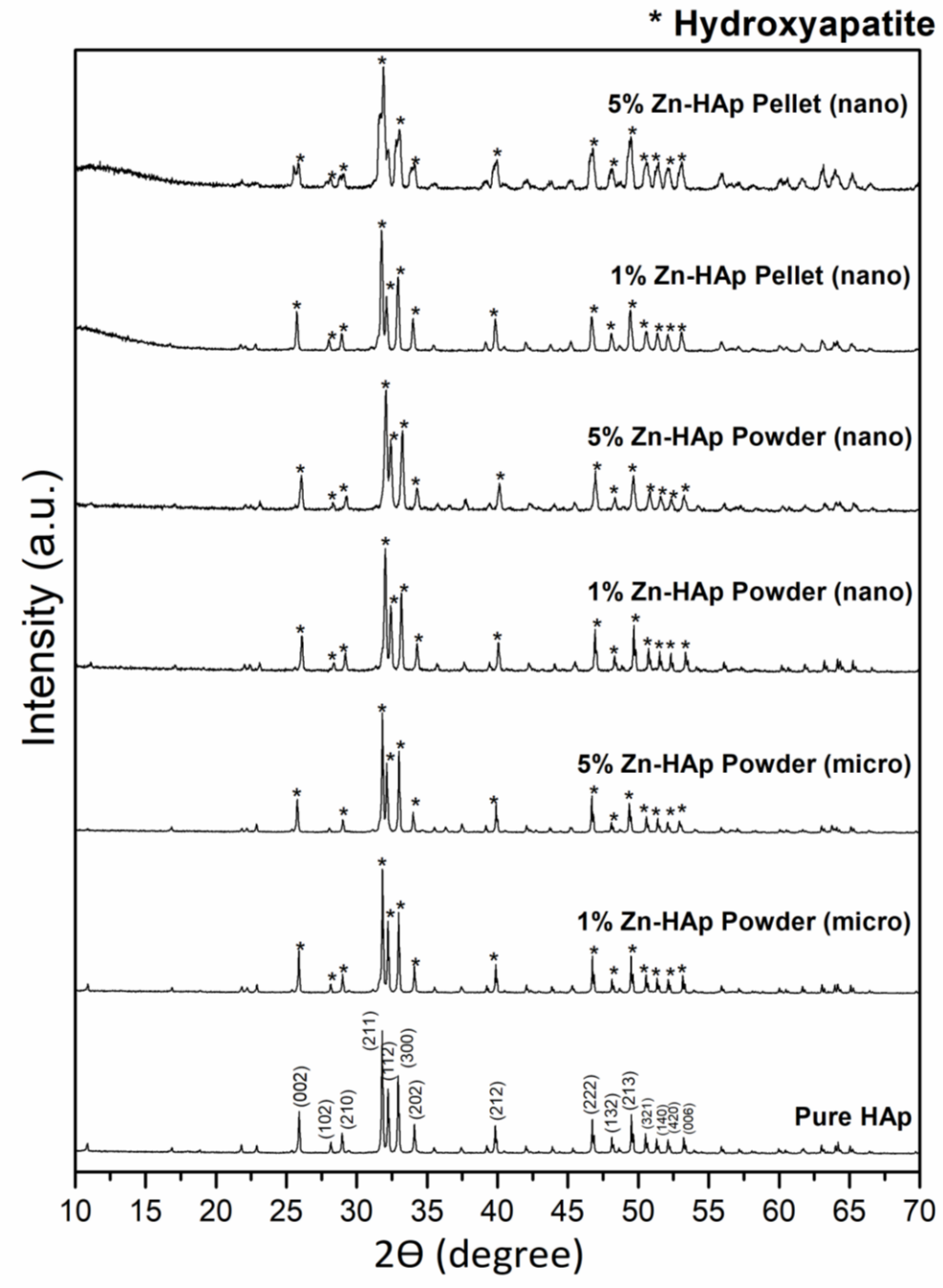

Figure 6.3 XRD analysis of hydroxyapatite powder doped with zinc with respect to different concentrations and particle sizes.

During the mixing process, zinc ions and nanoparticles are assumed to substitute calcium. Slight peak shifts can be seen in case of all the zinc doped HAp samples with respect to pure HAp sample. However according to Bigi et al. if a sample material contains zinc doping concentration higher than 25%, then only additional peaks can be seen and zinc plays an inhibitory role in the process of crystallization. This means that in such cases apatite phases might not be clearly visible [64]. In case of the present study, as zinc doping was done at a weight percentage of 1 and 5 only, identifying specific peaks for zinc is hard. However, it can be assumed that zinc has got incorporated into the hydroxyapatite lattice structure without interfering with the structural characteristics of pure HAp to produce zinc substituted hydroxyapatite.

6.1.4 XRD ANALYSIS OF COPPER DOPED HYDROXYAPATITE

Figure 6.4 contains diffraction patterns of – pure HAp powder, HAp powder doped with 1 weight percentage of copper of micro-particle size range, HAp powder doped with 5 weight percentage of copper of micro-particle size range, HAp powder doped with 1 weight percentage of copper of nanoparticle range, HAp powder doped with 5 weight percentage of copper of nanoparticle range, HAp pellet doped with 1 weight percentage of copper of nanoparticle range and HAp pellet doped with 5 weight percentage of copper of nanoparticle range. In figure 6.4, all the characteristics peaks of hydroxyapatite sintered at 1250°C can be identified as (002), (102), (210), (211), (112), (300), (202), (212), (222), (132), (213), (321), (140), (420) and (006). No major peak of any other substance such as bi-calcium phosphate (BCP), tri-calcium phosphate (TCP), tetra-calcium phosphate (TTCP) or calcium oxide can be seen in the patterns. The presence of CuO can be generally identified by the small peak present at $2\Theta = 38°$ (JCPDS no. 48-1548). In all the samples, a small peak can be seen in that position. All the samples were sintered at 1250°C and no other impurity patterns or secondary crystalline phases were identified in the x-ray diffraction pattern of the samples. This might indicate that the copper micro or nanoparticles have successfully or fully got incorporated into the apatite lattice structure, which can be called as copper substituted hydroxyapatite. Addition of copper makes no changes to the properties of the matrix of hydroxyapatite.

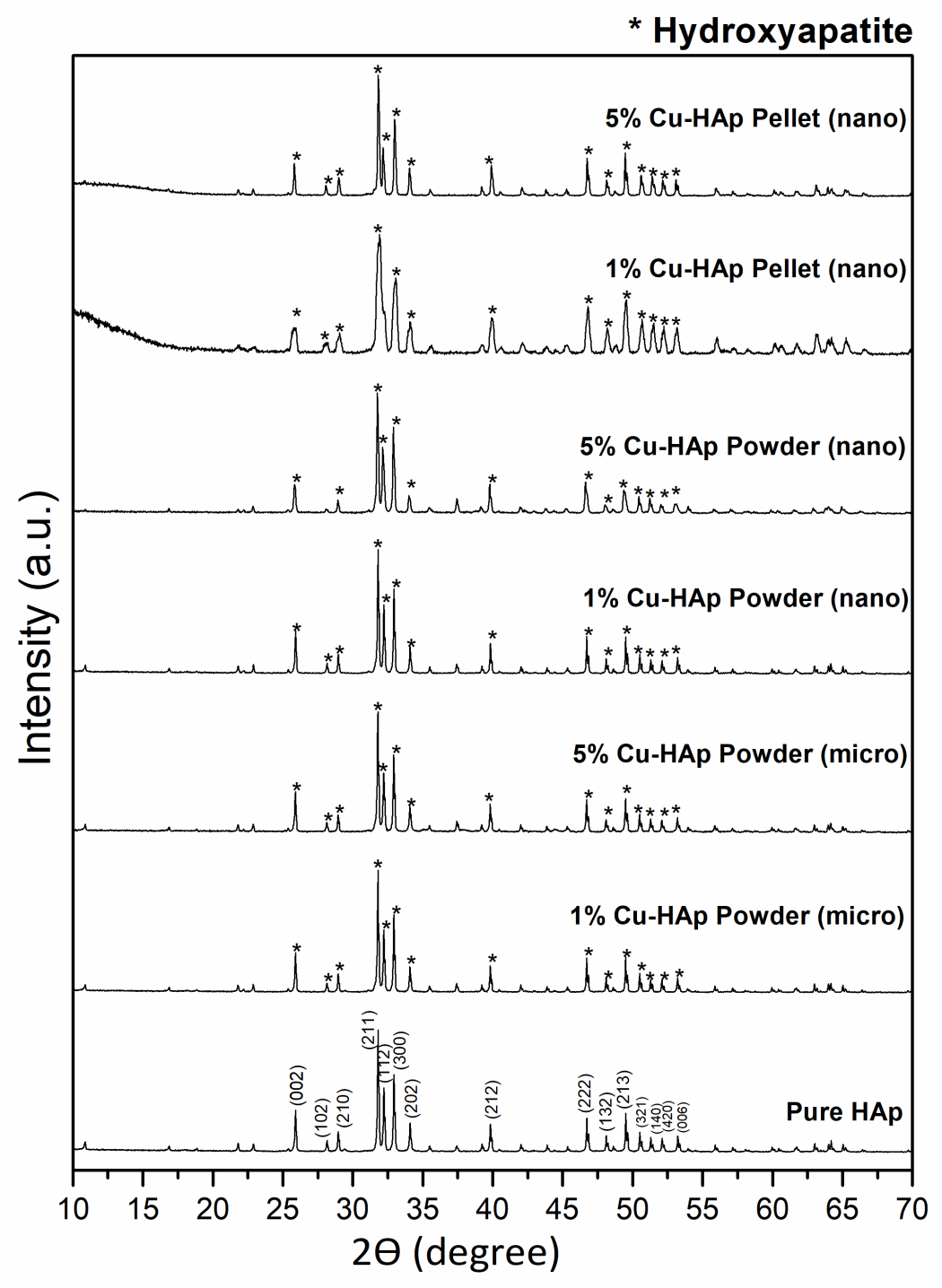

Figure 6.4 XRD analysis of hydroxyapatite powder doped with copper with respect to different concentrations and particle sizes.

6.2 ELEMENTAL COMPOSITIONAL ANALYSIS BY FOURIER TRANSFORM INFRARED SPECTROSCOPY OF PURE AND METAL OXIDE DOPED HYDROXYAPATITE POWDERS

6.2.1 FTIR ANALYSIS OF PURE HYDROXYAPATITE

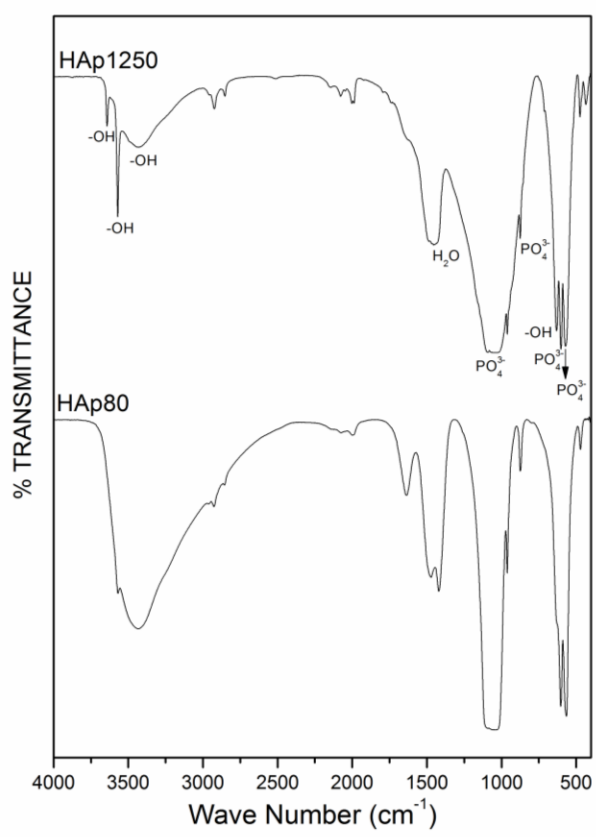

Figure 6.5 FTIR analysis of pure hydroxyapatite – dried at 80°C and sintered at 1250°C

FTIR analysis was done for hydroxyapatite powder dried at 80°C overnight inside a hot-air oven and for hydroxyapatite powder sintered at 1250°C for 2h inside a high temperature furnace. In case of both the samples, due to presence of water strong peaks can be seen at 3400 cm^{-1} and 1650 cm^{-1}. These water molecules could be identified due to the stretching and bending vibration of O—H bond. Characteristics phosphate groups or their corresponding peaks can be identified at 1090 cm^{-1}, 900 cm^{-1} and 550 cm^{-1}. In case of hydroxyapatite powder dried at 80°C, while the preparation stage, reaction might have taken place with atmospheric carbon di-oxide and therefore a peak can be seen at 870 cm^{-1}. In hydroxyapatite powder sintered at 1250°C, small

peaks seen at 3000 cm^{-1} and 2000 cm^{-1} might be due to C—H stretching and C—O stretching respectively.

6.2.2 FTIR ANALYSIS OF SILVER DOPED HYDROXYAPATITE

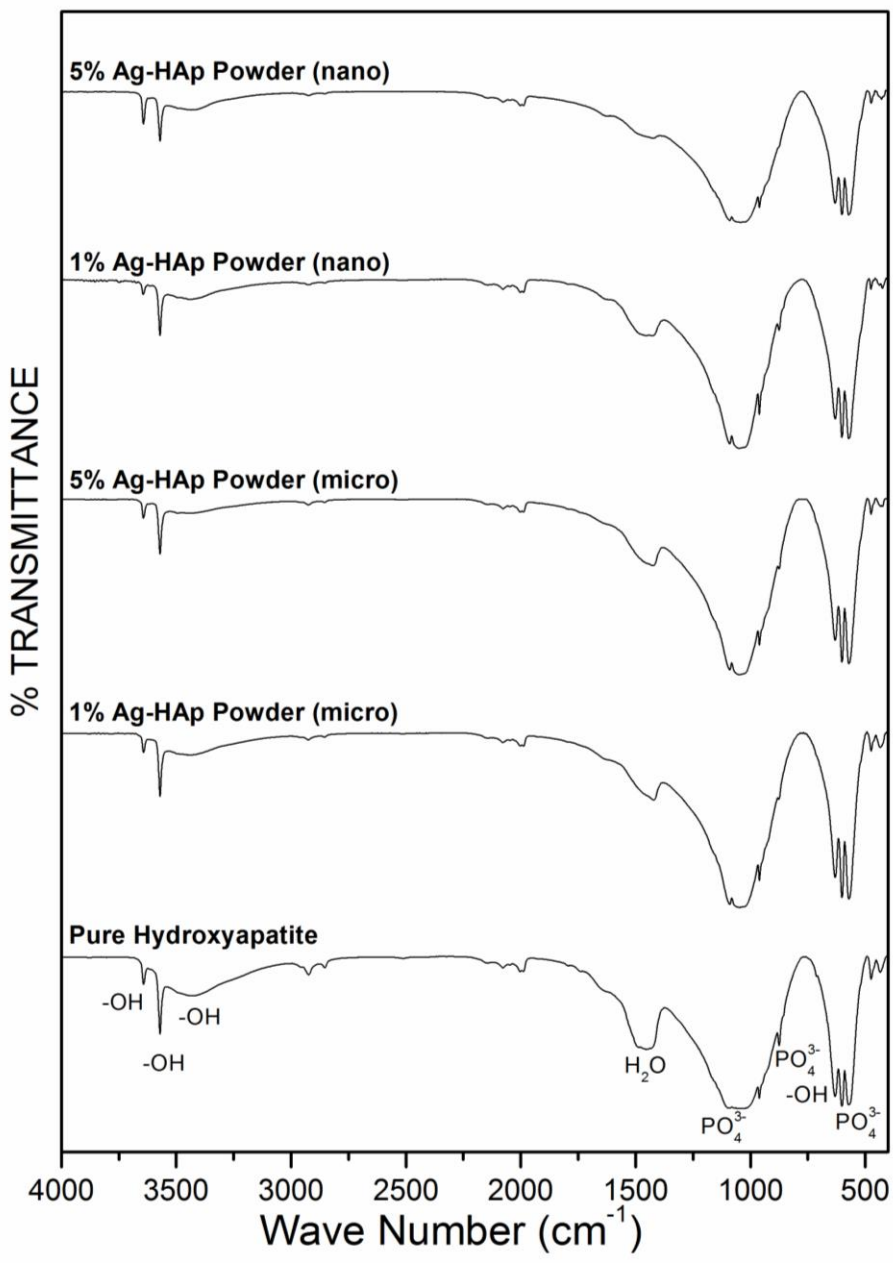

Figure 6.6 FTIR analysis of hydroxyapatite doped with silver in different concentrations and with different particle size

Figure 6.6 contains FTIR spectrum of pure hydroxyapatite sintered at 1250°C, hydroxyapatite doped with 1 weight percentage of silver in the micro particle size range, hydroxyapatite doped with 5 weight percentage of silver in the micro particle size range, hydroxyapatite doped with 1 weight percentage of silver in the nanoparticle range and hydroxyapatite doped with 5 weight percentage of silver in the nanoparticle range. In case of all the samples, due to presence of water strong peaks can be seen at 3400 cm^{-1} and 1650 cm^{-1}. These water molecules could be identified due to the stretching and bending vibration of O—H bond. Characteristics phosphate groups and their corresponding peaks can be identified at 1090 cm^{-1}, 900 cm^{-1} and 550 cm^{-1}. In all the samples small peaks seen at 3000 cm^{-1} and 2000 cm^{-1} might be due to C—H stretching and C—O stretching respectively. The FTIR spectrum of silver doped hydroxyapatite is almost exactly the same as the FTIR spectrum of pure hydroxyapatite. According to the data presented by Shirkhanzadeh et al. substitution by silver in the hydroxyapatite structure could not be detected by FTIR analysis as the substitution does not cause any structural change [65].

6.2.3 FTIR ANALYSIS OF ZINC DOPED HYDROXYAPATITE

Figure 6.7 contains FTIR spectrum of pure hydroxyapatite sintered at 1250°C, hydroxyapatite doped with 1 weight percentage of zinc in the micro particle size range, hydroxyapatite doped with 5 weight percentage of zinc in the micro particle size range, hydroxyapatite doped with 1 weight percentage of zinc in the nanoparticle range and hydroxyapatite doped with 5 weight percentage of zinc in the nanoparticle range. In case of all the samples, due to presence of water strong peaks can be seen at 3400 cm^{-1} and 1650 cm^{-1}. These water molecules could be identified due to the stretching and bending vibration of O—H bond. Characteristics phosphate groups and their corresponding peaks can be identified at 1090 cm^{-1}, 900 cm^{-1} and 550 cm^{-1}. In all the samples small peaks seen at 3000 cm^{-1} and 2000 cm^{-1} might be due to C—H stretching and C—O stretching respectively. The FTIR spectrum of zinc doped hydroxyapatite is almost exactly the same as the FTIR spectrum of pure hydroxyapatite. Substitution by zinc in the hydroxyapatite structure could not be detected by FTIR analysis as the substitution does not cause any structural change.

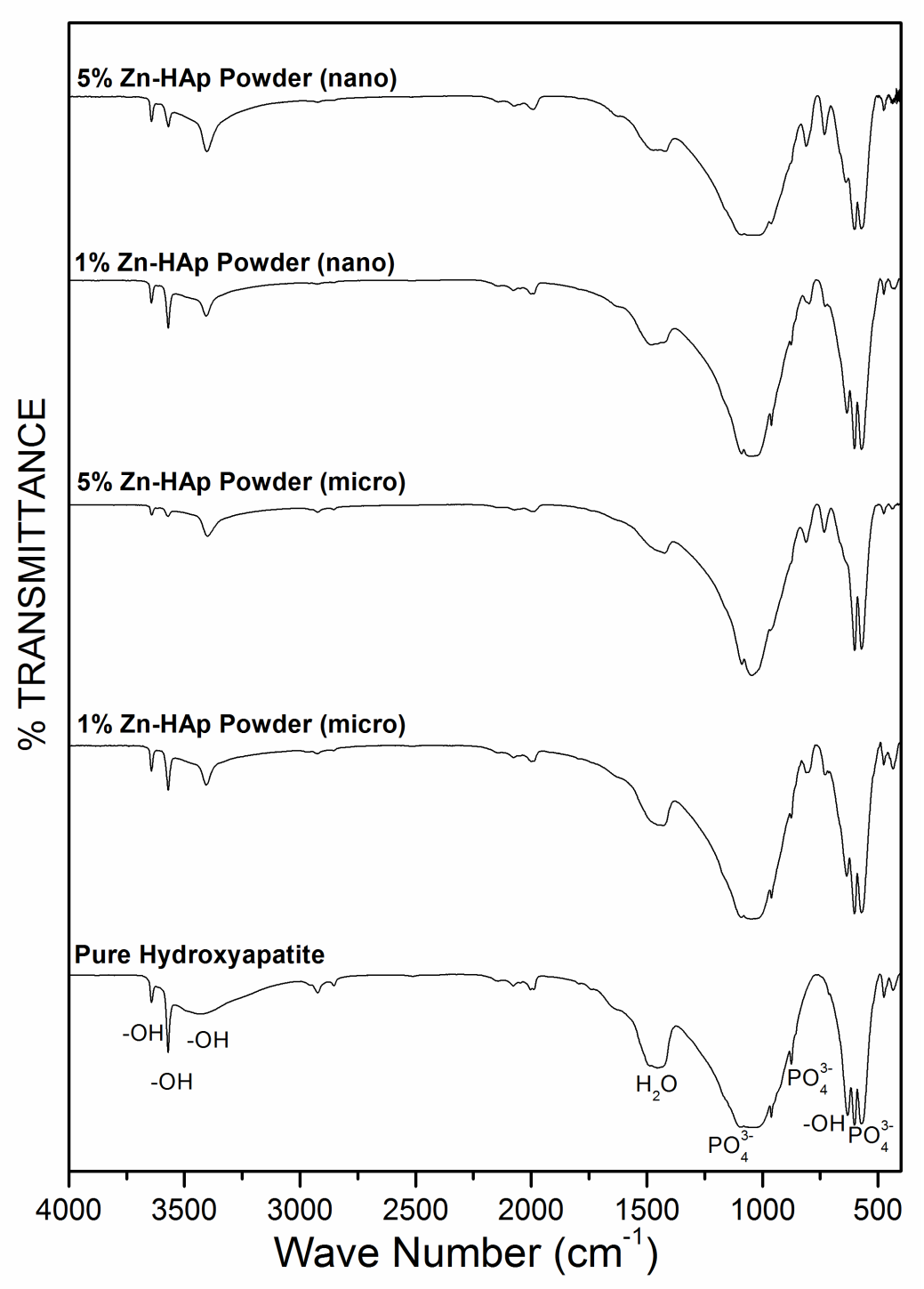

Figure 6.7 FTIR analysis of hydroxyapatite doped with zinc in different concentrations and with different particle size

6.2.4 FTIR ANALYSIS OF COPPER DOPED HYDROXYAPATITE

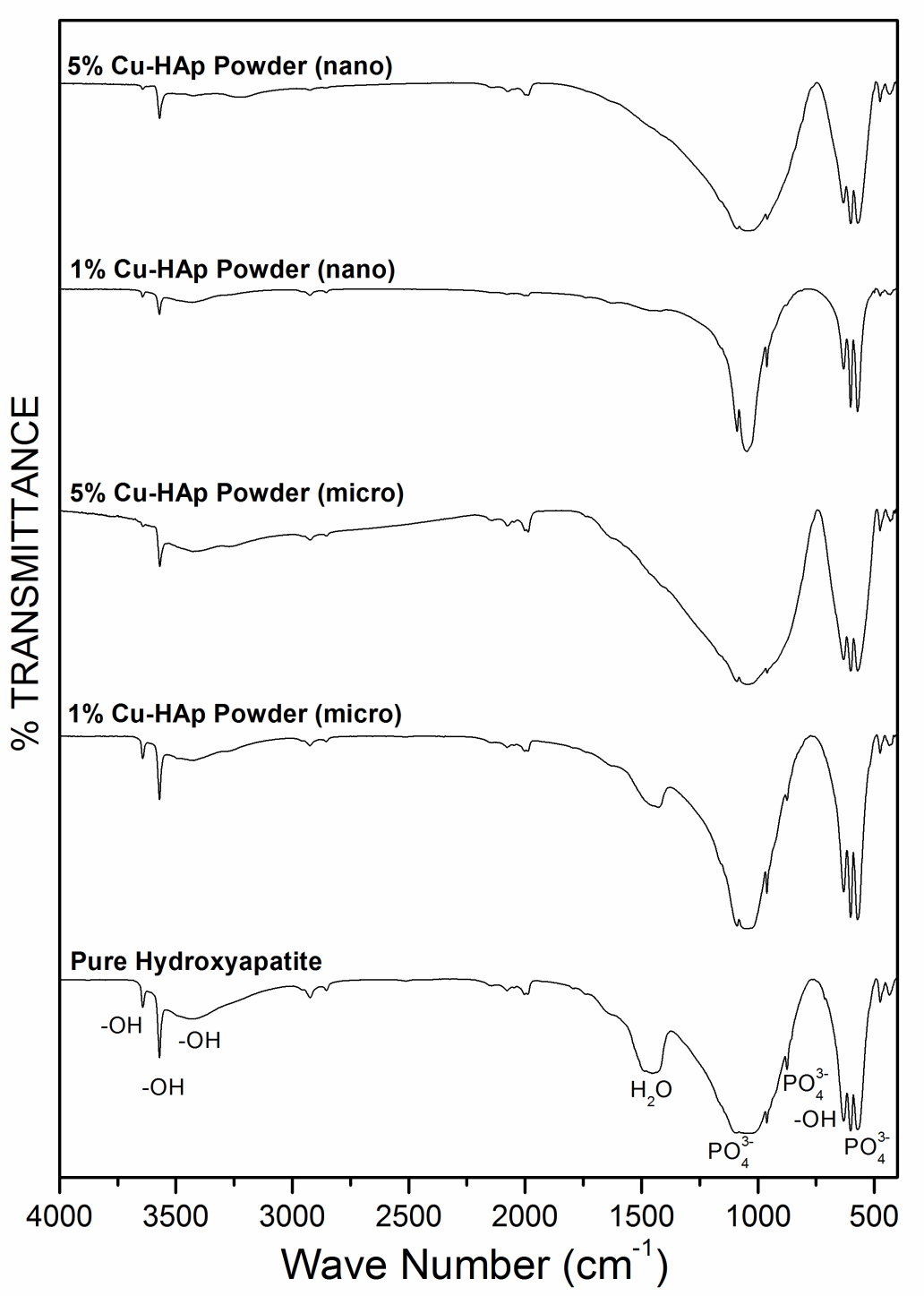

Figure 6.8 FTIR analysis of hydroxyapatite doped with copper in different concentrations and with different particle size

Figure 6.8 contains FTIR spectrum of pure hydroxyapatite sintered at 1250°C, hydroxyapatite doped with 1 weight percentage of copper in the micro particle size range, hydroxyapatite doped with 5 weight percentage of copper in the micro particle size range, hydroxyapatite doped with 1 weight percentage of copper in the nanoparticle range and hydroxyapatite doped with 5 weight percentage of copper in the nanoparticle range. In case of all the samples, due to presence of water strong peaks can be seen at 3400 cm^{-1} and 1650 cm^{-1}. These water molecules could be identified due to the stretching and bending vibration of O—H bond. Characteristics phosphate groups and their corresponding peaks can be identified at 1090 cm^{-1}, 900 cm^{-1} and 550 cm^{-1}. In all the samples small peaks seen at 3000 cm^{-1} and 2000 cm^{-1} might be due to C—H stretching and C—O stretching respectively. The FTIR spectrum of copper doped hydroxyapatite is almost exactly the same as the FTIR spectrum of pure hydroxyapatite. Substitution by copper in the hydroxyapatite structure could not be detected by FTIR analysis as the substitution does not cause any structural change.

6.3 SURFACE MICROSTRUCTURE ANALYSIS BY FIELD EMISSION SCANNING ELECTRON MICROSCOPY OF PURE AND METAL OXIDE DOPED HYDROXYAPATITE POWDERS

6.3.1 SURFACE MICROSTRUCTURE ANALYSIS OF PURE HYDROXYAPATITE

Figure 6.9 contains field emission scanning electron microscopy images of pure hydroxyapatite at four different magnifications which are – 500x, 2000x, 5000x and 10000x. Pellets were made from pure hydroxyapatite powder using a hydraulic press at 2000 psi pressure. The sample was carbon coated prior inserting into the machine. The upper left picture captured at 500x magnification shows a broad area of the hydroxyapatite surface which is smooth as well as does not have any cracks. In 2000x magnification, the upper right image, the same area can be seen more clearly. Pores are visible to a certain extent at this stage. In 5000x magnification the porous surface of the sample is clearly visible. Looking at the surface it can be considered that the hydroxyapatite powder or the pellet possesses very low density and high porosity. In 10000x magnification, the lower right image, pores are clearly visible and the pores can measured to

have diameters of 1 to 1.5 nanometers. Due to this highly porous nature of hydroxyapatite, dopants can easily bind to improve its various characteristics.

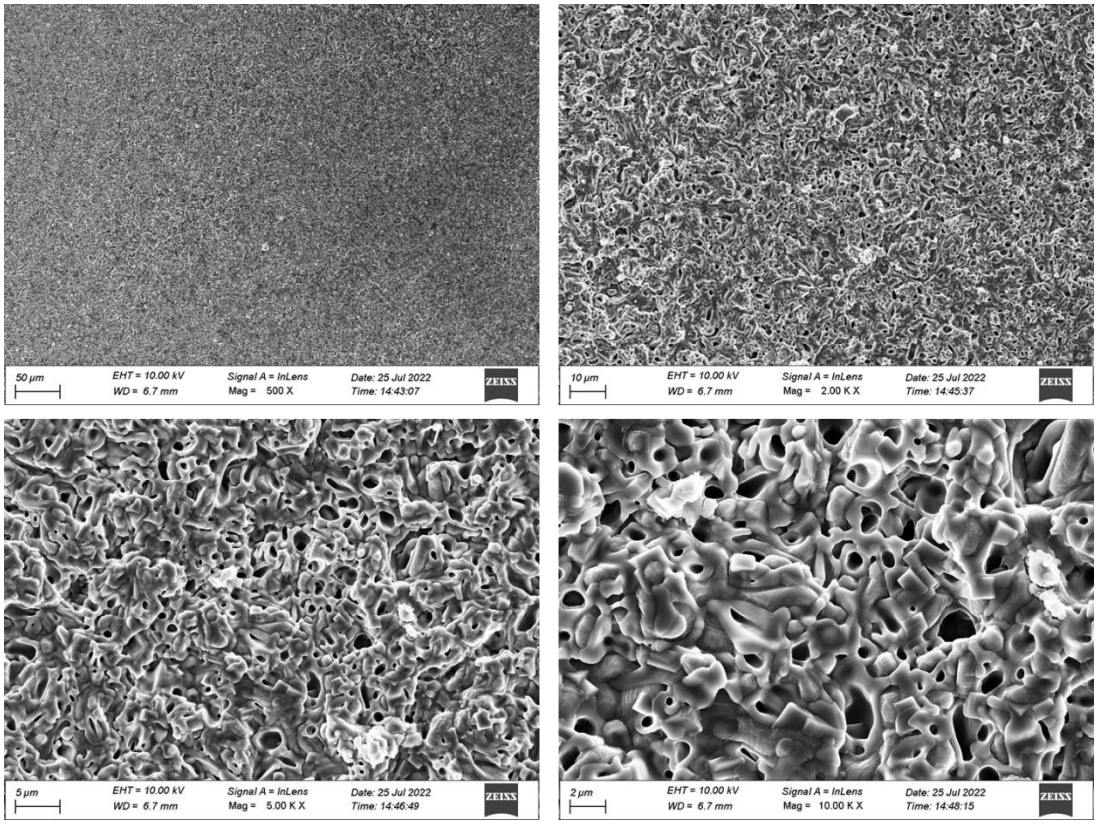

Figure 6.9 FESEM images of pure hydroxyapatite pellets captured at four different magnifications

6.3.2 SURFACE MICROSTRUCTURE ANALYSIS OF SILVER DOPED HYDROXYAPATITE

Figure 6.10 contains field emission scanning electron microscopy images of pure hydroxyapatite doped with silver nanoparticles at 1 weight percentage and 5 weight percentage at four different magnifications which are – 500x, 2000x, 5000x and 10000x. Pellets were made from pure hydroxyapatite powder doped with two different concentrations of silver using a hydraulic press at 2000 psi pressure. The samples were carbon coated prior inserting into the machine. Figure 6.10.A contains FESEM images of 1% silver doped HAp sample and figure 6.10.B contains FESEM images of 5% silver doped HAp sample.

In case of picture-group A, the upper left picture captured at 500x magnification shows a broad area of the pellet surface which looks to be rough with certain irregularities. In 2000x magnification, the upper right image, the same area can be seen more clearly. Pores are not at all visible at this stage. The surface composition looks dense. In 5000x magnification the dense surface of the sample is clearly visible. The grains of the material can be seen at this magnification. In 10000x magnification, the lower right image, it is clear that there are no pores present in the structure. The silver molecules have firmly or strongly bound to the hydroxyapatite molecules to increase its crystallinity. This binding can be considered to be very stable by looking at the images.

In case of picture-group B, the upper left picture captured at 500x magnification shows a broad area of the pellet surface which looks to be rough with certain cracks. In 2000x magnification, the upper right image, the same area can be seen more clearly. Pores are not visible as they were seen in case of pure hydroxyapatite at this stage. The surface composition looks dense. However certain cracks or holes are clearly visible. In 5000x magnification the dense surface of the sample is clearly visible. It is conclusive that doping hydroxyapatite with silver nanoparticles and then heat treating it at 1250°C has increased the density and reduced the porosity as compared to pure hydroxyapatite sample. The densely packed grains are clearly visible. In 10000x magnification, the lower right image, it is clear that there are no pores present in the structure. The silver molecules have firmly or strongly bound to the hydroxyapatite molecules to increase its crystallinity and stability.

A

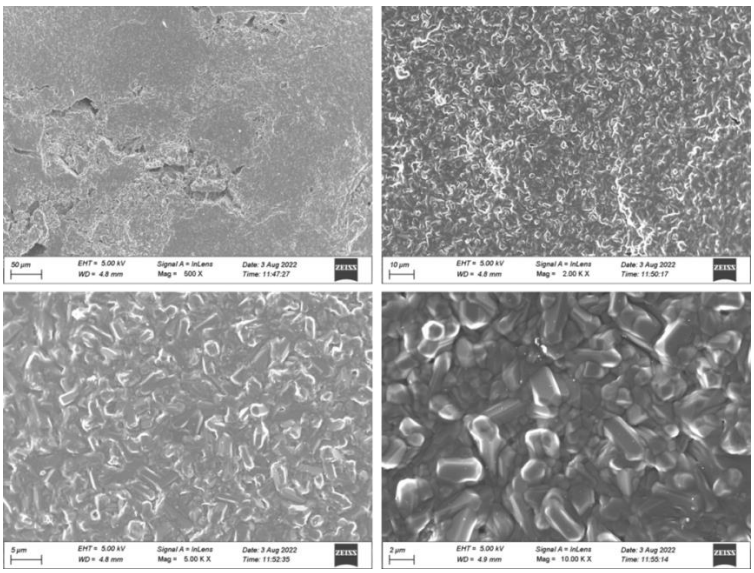

B

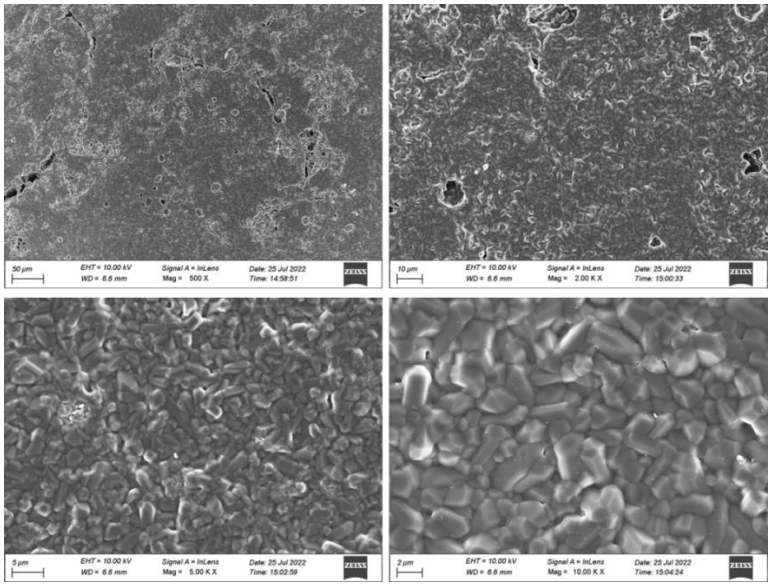

Figure 6.10 FESEM images of pure hydroxyapatite doped with silver nanoparticles (A) at 1 weight percentage and (B) at 5 weight percentage

6.3.3 SURFACE MICROSTRUCTURE ANALYSIS OF ZINC DOPED HYDROXYAPATITE

Figure 6.11 contains field emission scanning electron microscopy images of pure hydroxyapatite doped with zinc nanoparticles at 1 weight percentage and 5 weight percentage at four different magnifications which are – 500x, 2000x, 5000x and 10000x. Pellets were made from pure hydroxyapatite powder doped with two different concentrations of zinc using a hydraulic press at 2000 psi pressure. The samples were carbon coated prior inserting into the machine. Figure 6.11.A contains FESEM images of 1% zinc doped HAp sample and figure 6.11.B contains FESEM images of 5% zinc doped HAp sample.

In case of picture-group A, the upper left picture captured at 500x magnification shows a broad area of the pellet surface which looks to be rough with visible cracks. In 2000x magnification, the upper right image, the same area can be seen more clearly. Pores are not at all visible at this stage. Slight cracks can be seen at the upper right coner. The surface composition looks dense. In 5000x magnification the dense surface of the sample is clearly visible. The grains of the material can be seen at this magnification. A few pores can also be seen. In 10000x magnification, the

lower right image, it is clear some pores are present in the structure. The zinc molecules have firmly or strongly bound to the hydroxyapatite molecules to increase its crystallinity. The bound grains are clearly visible. This binding can be considered to be very stable by looking at the images.

In case of picture-group B, the upper left picture captured at 500x magnification shows a broad area of the pellet surface which looks to be rough with a few cracks. In 2000x magnification, the upper right image, the same area can be seen more clearly. A few pores are visible as they were seen in case of pure hydroxyapatite at this stage. The surface composition looks dense. In 5000x magnification the dense surface of the sample is clearly visible. It is conclusive that doping hydroxyapatite with zinc nanoparticles and then heat treating it at 1250°C has increased the density and reduced the porosity as compared to pure hydroxyapatite sample. The densely packed grains are clearly visible. In 10000x magnification, the lower right image, it is seen that a few pores are present in the structure. Presence of more number of pores compared to silver doped hydroxyapatite might indicate that zinc doped samples have less density than those doped with silver.

A

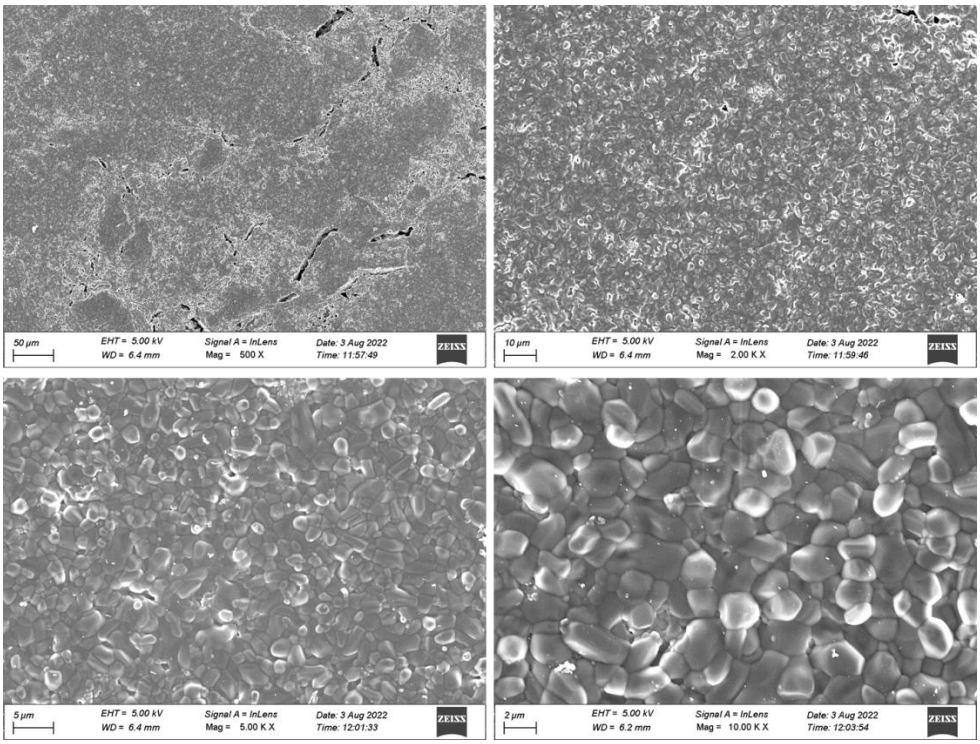

B

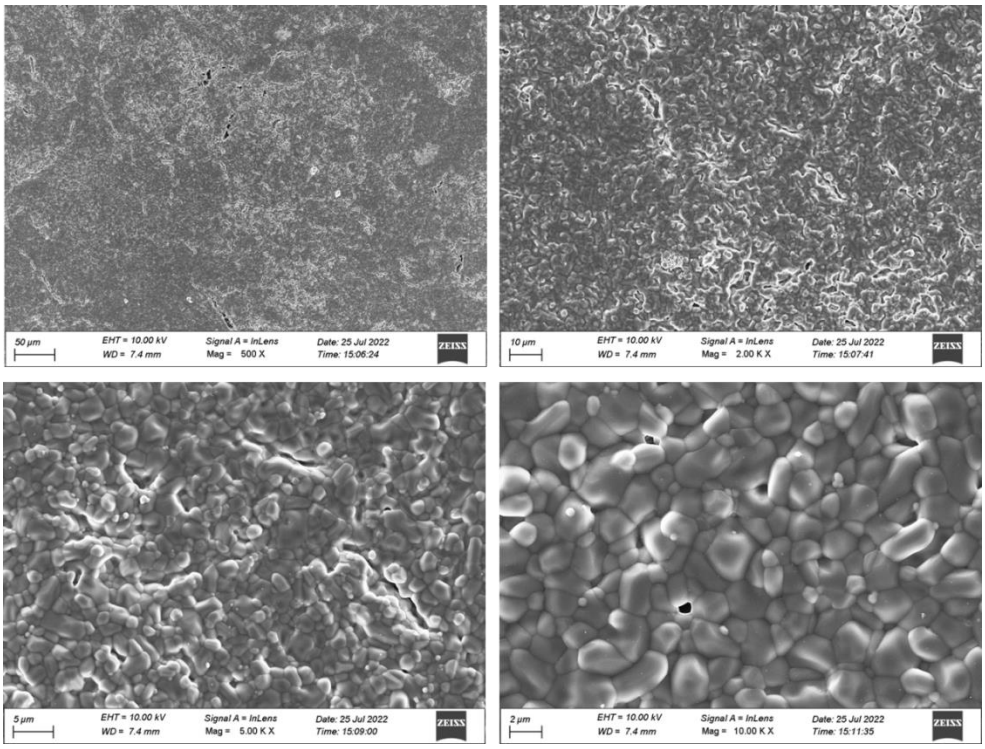

Figure 6.11 FESEM images of pure hydroxyapatite doped with zinc nanoparticles (A) at 1 weight percentage and (B) at 5 weight percentage

6.3.4 SURFACE MICROSTRUCTURE ANALYSIS OF COPPER DOPED HYDROXYAPATITE

Figure 6.12 contains field emission scanning electron microscopy images of pure hydroxyapatite doped with copper nanoparticles at 1 weight percentage and 5 weight percentage at four different magnifications which are – 500x, 2000x, 5000x and 10000x. Pellets were made from pure hydroxyapatite powder doped with two different concentrations of copper using a hydraulic press at 2000 psi pressure. The samples were carbon coated prior inserting into the machine. Figure 6.12.A contains FESEM images of hydroxyapatite powder doped with 1 weight percentage of copper nanoparticles and figure 6.12.B contains FESEM images of hydroxyapatite powder doped with 5 weight percentage of copper nanoparticles.

In case of picture-group A, the upper left picture captured at 500x magnification shows a broad area of the pellet surface which looks to be smooth without any visible irregularities or cracks. In

2000x magnification, the upper right image, the same area can be seen more clearly. Pores are not clearly visible at this stage. One tiny crack and another pore can be seen on the surface. The surface composition looks dense. In 5000x magnification the dense surface of the sample is clearly visible. The grains of the material can be seen at this magnification. Only a few pores can be seen. In 10000x magnification, the lower right image, it is clear some pores are present in the structure. The copper molecules have firmly or strongly bound to the hydroxyapatite molecules to increase its crystallinity. The bound grains are clearly visible. This binding can be considered to be very stable by looking at the images.

In case of picture-group B, the upper left picture captured at 500x magnification shows a broad area of the pellet surface which looks to be relatively smooth without any cracks. In 2000x magnification, the upper right image, the same area can be seen more clearly. Pores are not at all visible as they were seen in case of pure hydroxyapatite at this stage. The surface composition looks dense. In 5000x magnification the dense surface of the sample is clearly visible. It is conclusive that doping hydroxyapatite with copper nanoparticles and then heat treating it at 1250°C has increased the density and reduced the porosity as compared to pure hydroxyapatite sample. The densely packed grains are clearly visible. In 10000x magnification, the lower right image, it is seen that a few pores are present in the structure. The copper molecules have firmly or strongly bound to the hydroxyapatite molecules to increase its crystallinity and stability. Due to the presence of few pores in the structure and dense grain arrangement, copper doped hydroxyapatite might possess same mechanical properties as compared to silver doped hydroxyapatite.

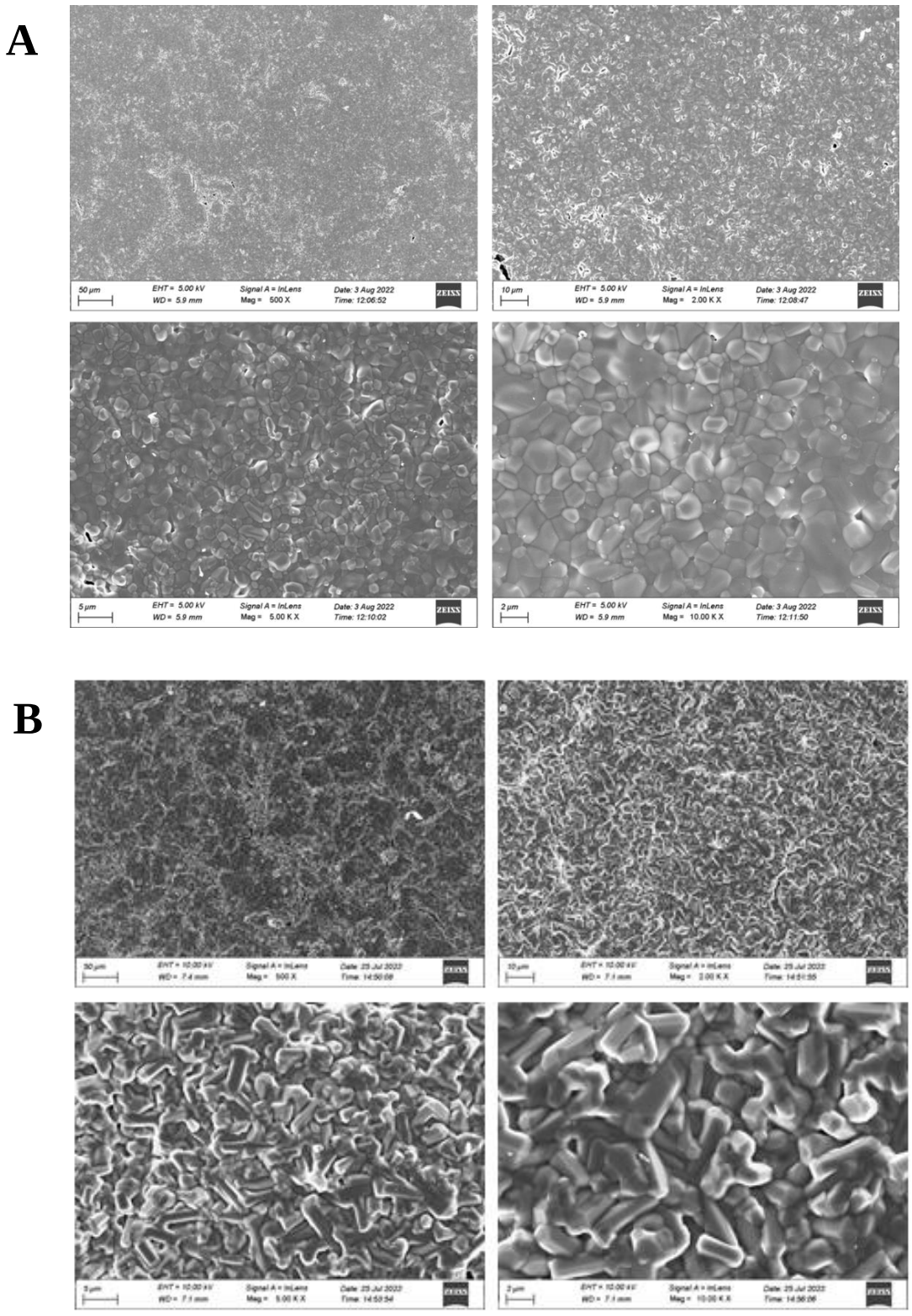

Figure 6.12 FESEM images of pure hydroxyapatite doped with copper nanoparticles (A) at 1 weight percentage and (B) at 5 weight percentage

6.4 IN VITRO ASSESSMENT OF ANTIBACTERIAL EFFICACY OF PURE AND METAL OXIDE DOPED HYDROXYAPATITE POWDERS

6.4.1 IN VITRO ASSESSMENT OF ANTIBACTERIAL EFFICACY OF PURE AND MICRO-SIZED METAL OXIDE POWDER DOPED HYDROXYAPATITE POWDERS (DOPANTS – Ag, Zn and Cu)

In this antibacterial study, antibacterial efficacy of pure hydroxyapatite powder along with all the doped samples – silver, zinc and copper, in their micro-particle size range at 1 and 5 weight percentages were checked against *E. coli*, a gram negative bacterial. All the samples were tested at powder form and three different concentrations were selected to treat the bacteria. The selected concentrations were 5 mg/mL, 10 mg/mL and 20 mg/mL. Bacteria without any treatment were taken as the negative control and bacteria treated with streptomycin, an antibiotic were taken as the positive control. In case of pure hydroxyapatite, 100% growth of bacteria was seen for all the three concentrations as hydroxyapatite does not possess any antibacterial properties in its natural or pure state.

The best results were obtained in case of copper doped hydroxyapatite samples. Both 1 weight percent and 5 weight percent copper doped hydroxyapatite samples at 20 mg/mL concentration showed optimum antibacterial activity. 20 mg/mL concentration of 5 weight percent copper doped hydroxyapatite powder showed antibacterial efficacy same as the antibiotic or the positive control. 100% inhibition of bacterial growth was seen in this case. In case of 20 mg/mL concentration of 1 weight percent copper doped hydroxyapatite sample, growth of only a few bacterial colonies were seen. Almost 80% inhibition of bacterial growth was seen in case of 1 weight percent copper doped hydroxyapatite sample. Again in case of 10 mg/mL concentration of 5 weight percent copper doped hydroxyapatite sample, a little inhibition in bacterial growth can be seen. Approximately 10% inhibition of bacterial growth is visible here. However, the other concentrations – 10 mg/mL of 1 weight percent copper doped hydroxyapatite, 5 mg/mL of 5 and 1 weight percent copper doped hydroxyapatite samples did not show any antibacterial activity on the bacteria.

Silver and zinc doped hydroxyapatite samples did not show any antibacterial activity in any of their concentrations. Zinc ions are known to have antibacterial properties at a higher level. It

might be possible that even 20 mg/mL concentration of zinc doped hydroxyapatite powder is not enough for zinc to show antibacterial activity on the bacteria. Silver is very popularly used as antibacterial agent. In our case silver oxide was used to dope hydroxyapatite powder. Silver oxide is not known to have any antibacterial properties. This might be the reason why silver doped hydroxyapatite powder did not show any antibacterial activity at any of the concentrations.

Among all the three micro particle sized dopants – silver, zinc and copper, copper doped hydroxyapatite powder has shown the best results.

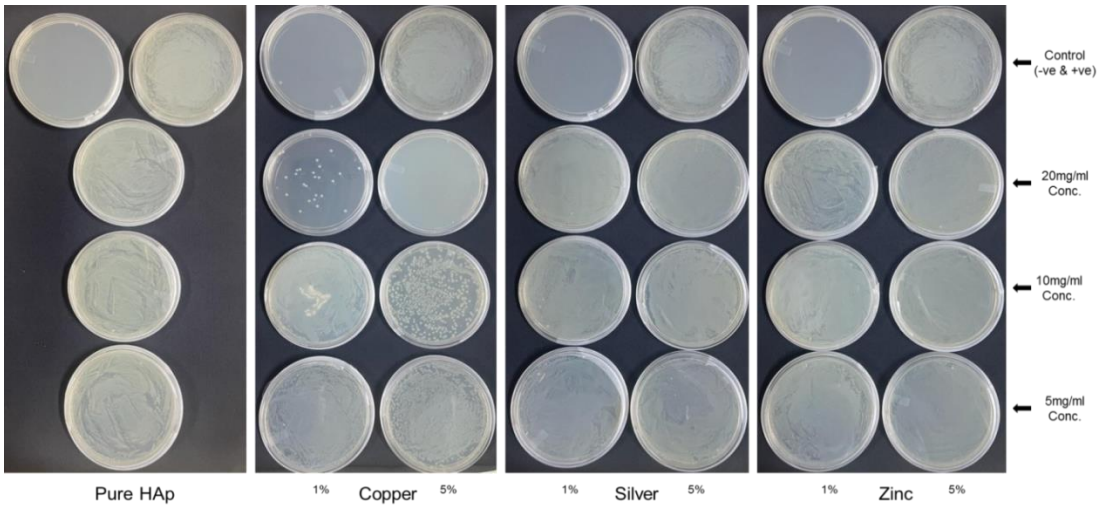

Figure 6.13 Antibacterial efficacy of pure and micro-sized metal oxide powder doped hydroxyapatite powders at different concentration against *E. coli*

6.4.2 IN VITRO ASSESSMENT OF ANTIBACTERIAL EFFICACY OF PURE AND NANO-SIZED METAL OXIDE POWDER DOPED HYDROXYAPATITE POWDERS (DOPANTS – Ag, Zn and Cu)

In this antibacterial study, antibacterial efficacy of pure hydroxyapatite powder along with all the doped samples – silver, zinc and copper, in their nanoparticle size range at 1 and 5 weight percentages were checked against *E. coli*, gram negative bacterial. All the samples were tested at powder form and three different concentrations were selected to treat the bacteria. The selected concentrations were 5 mg/mL, 10 mg/mL and 20 mg/mL. Bacteria without any treatment were

taken as the negative control and bacteria treated with streptomycin (antibiotic) were taken as the positive control. In case of pure hydroxyapatite, 100% growth of bacteria was seen for all the three concentrations as hydroxyapatite does not possess any antibacterial properties in its natural or pure state.

In this test also, copper doped hydroxyapatite powder samples showed the best results. 20 mg/mL concentration of both 1 and 5 weight percent copper doped hydroxyapatite samples showed 100% inhibition of bacterial growth. The antibacterial efficacy of both these samples at this concentration is equal to that of streptomycin. 10 mg/mL concentration of 5 weight percent copper doped hydroxyapatite sample showed almost 20% bacterial growth inhibition. However the other concentrations of 1 and 5 weight percent copper doped hydroxyapatite samples did not show any antibacterial efficacy. In case of silver and zinc nanoparticle doped hydroxyapatite powders, antibacterial efficacy can be seen in each case. 1 weight percent of both silver and zinc doped hydroxyapatite could not show much antibacterial properties. Only a little bacterial growth inhibition could be seen. In case of 5 weight percent of silver and zinc doped hydroxyapatite powders, both the samples showed almost the same antibacterial activity in each concentration. None of these two dopants could inhibit the bacterial growth at 100%. In comparison, copper doped hydroxyapatite samples show best antibacterial activity in the nanoparticle size range with respect to silver and zinc.

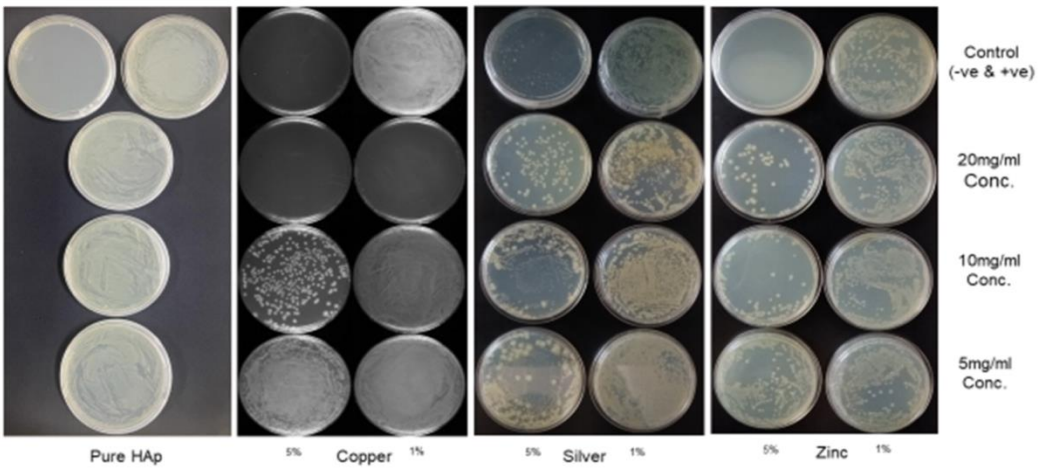

Figure 6.14 Antibacterial efficacy of pure and nano-sized metal oxide powder doped hydroxyapatite powders at different concentrations against *E. coli*

CONCLUSION

1. Pure hydroxyapatite powder was successfully synthesized.

2. All the three dopants in their micro and nanoparticle range were successfully mixed with hydroxyapatite powder.

3. All the physico-chemical analysis – phase analysis by x-ray diffraction, elemental analysis by FTIR spectroscopy, surface microstructure analysis by FESEM – were successfully conducted.

4. With respect to antibacterial properties, all the dopants in their nanoparticle range showed higher antibacterial efficacy.

5. Silver and zinc in micro-particle size range doped hydroxyapatite samples showed little antibacterial efficacy.

6. Silver and zinc in their nanoparticle range doped hydroxyapatite powders showed moderate antibacterial efficacy.

7. Dopants' chemical state is very much important to get any antibacterial property. As silver was in oxide form it did not provide any antibacterial property which is very much prominent as per reports when it is in ionic form.

8. Copper doped hydroxyapatite powders showed highest antibacterial efficacy compared to silver and zinc doped hydroxyapatite powders.

9. Copper in its nanoparticle range doped hydroxyapatite powder showed the best antibacterial efficacy.

7.1 FUTURE PROSPECTIVE

All the samples in their nanoparticle range can be tested for cytotoxicity assays such as MTT assay. MTT assay can be done to ascertain if any of the samples possesses any cytotoxicity. As silver, zinc and copper are present in the human body at trace quantities; higher exposure of these dopants to cells might be toxic. Along with cytotoxicity, cell morphology studies can also

be conducted using these powder samples. DAPI – FITC staining method can be used to analyze cell morphology when cells come into contact with these powder samples. Along with these, to obtain a quantitative analysis of antibacterial efficacy of the samples, a zone of inhibition study can be done.

Another approach can be to reduce the weight percentage of the dopants further from those which have been used in this study (1 and 5 weight percent of dopants), if these samples show any cytotoxicity. Lower weight percentages can be used such as 0.25, 0.5, 0.75 weight percentages etc. In order to obtain better results hydroxyapatite can be thought of to be doped with more than one dopant. A combination of different dopants and different concentrations can be used to dope hydroxyapatite to obtain optimum antibacterial as well as physico-chemical properties.

REFERENCES

[1] L.L. Hench, Bioceramics: from concept to clinic, J. Am. Ceram. Soc. 74 (1991) 1487–1510, https://doi.org/10.1111/j.1151-2916.1991.tb07132.x.

[2] R.Z. LeGeros, Properties of osteoconductive biomaterials: calcium phosphates: Clin. Orthop. 395 (2002) 81–98, https://doi.org/10.1097/00003086-200202000- 00009.

[3] M.P. Ginebra, T. Traykova, J.A. Planell, Calcium phosphate cements as bone drug delivery systems: a review, J. Contr. Release 113 (2006) 102–110, https://doi.org/ 10.1016/j.jconrel.2006.04.007.

[4] L. Sun, C.C. Berndt, K.A. Gross, A. Kucuk, Material fundamentals and clinical performance of plasma-sprayed hydroxyapatite coatings: a review, J. Biomed. Mater. Res. 58 (2001) 570–592, https://doi.org/10.1002/jbm.1056.

[5] U. Heise, J.F. Osborn, F. Duwe, Hydroxyapatite ceramic as a bone substitute, Int. Orthop. 14 (1990), https://doi.org/10.1007/BF00178768.

[6] W. Chen, Y. Liu, H.S. Courtney, M. Bettenga, C.M. Agrawal, J.D. Bumgardner, J.L. Ong, In vitro anti-bacterial and biological properties of magnetron co-sputtered silver-containing hydroxyapatite coating, Biomaterials 27 (2006) 5512–5517.

[7] F. Heidenau, W. Mittelmeier, R. Detsch, M. Haenle, F. Stenzel, G. Ziegler, H. Gollwitzer, A novel antibacterial titania coating: metal ion toxicity and in vitro surface colonization, J. Mater. Sci. Mater. Med. 16 (2005) 883–888.

[8] R.J. Chung, M.F. Hsieh, C.W. Huang, L.H. Perng, H.W. Wen, T.S. Chin, Antimicrobial effects and human gingival biocompatibility of hydroxyapatite sol–gel coatings, J. Biomed. Mater. Res. B 76 (2006) 169–178.

[9] R. Kumar, H. Munstedt, Biomaterials 26 (2005) 2081–2088.

[10] C. Damm, H. Munstedt, A. Rosch, Mater. Chem. Phys. 108 (2008) 61–66.

[11] R. Langer, Biomaterials in drug delivery and tissue engineering: one laboratory's experience, Acc. Chem. Res. 33 (2000) 94–101.

[12] L.J. Bonassar, C.A. Vacanti, Tissue engineering: The first decade and beyond, J. Cell Biochem. 72 (1998) 97–303.

[13] K. Balagangadharan, S. Dhivya, N. Selvamurugan, Chitosan based nanofibers in bone tissue engineering, Int. J. Biol. Macromol. 104 (2017) 1372–1382, https:// doi.org/10.1016/j.ijbiomac.2016.12.046.

[14] S.Z. Fu, P.Y. Ni, B.Y. Wang, B.Y. Chu, L. Zheng, F. Luo, J.C. Luo, Z.Y. Qian, Injectable and thermo-sensitive PEG-PCL-PEG copolymer/collagen/n-HA hydrogel composite for guided bone regeneration, Biomaterials. 33 (2012) 4801–4809, https://doi.org/10.1016/j.biomaterials.2012.03.040.

[15] K.-T. Lim, D.K. Patel, H.W. Choung, H. Seonwoo, J. Kim, J.H. Chung, Evaluation of Bone Regeneration Potential of Long-Term Soaked Natural Hydroxyapatite, ACS Appl. Bio Mater. 12 (2019), https://doi.org/10.1021/acsabm.9b00345.

[16] C. Wang, D. Liu, C. Zhang, J. Sun, W. Feng, S.W. Xing-Jie Liang, J. Zhang, Defect-Related Luminescent Hydroxyapatite-Enhanced Osteogenic Differentiation of Bone Mesenchymal Stem Cells Via an ATP-Induced cAMP/PKA Pathway, ACS Appl. Mater. Interfaces. 8 (2016) 11262–11271, https://doi.org/10.1021/ acsami.6b01103.

[17] V. Singh, Medicinal plants and bone healing, Natl. J. Maxillofac. Surg. 8 (2017) 4–11, https://doi.org/10.4103/0975-5950.208972.

[18] K. Rezwana, Q.Z. Chena, J.J. Blakera, A.R. Boccaccini, Biodegradable and bioactive porous polymer/inorganic composite scaffolds for bone tissue engineering, Biomaterials. 27 (2006) 3413–3431, https://doi.org/10.1016/j. biomaterials.2006.01.039.

[19] R. del Campo, B. Savoini, L. Jordao, A. Mu˜noz, M.A. Monge, Cytocompatibility, biofilm assembly and corrosion behavior of Mg-HAP composites processed by extrusion, Mater. Sci. Eng. C. 78 (2017) 667–673, https://doi.org/10.1016/j. msec.2017.04.143.

[20] J. Anita Lett, M. Sundareswari, K. Ravichandran, B. Latha, S. Sagadevan, Fabrication and characterization of porous scaffolds for bone replacements using gum tragacanth, Mater. Sci. Eng. C. 96 (2019) 487–495, https://doi.org/ 10.1016/j.msec.2018.11.082.

[21] D.S. Gomes, A.M.C. Santos, G.A. Neves, R.R. Menezes, C. Grande, C. Grande, A brief review on hydroxyapatite production and use in biomedicine (Uma breve revis˜ao sobre a obtenç˜ao de hidroxiapatita e aplicaç˜ao na biomedicina), Cerˆamica. 65 (2019) 282–302.

[22] G. Ma, X.Y. Liu, Hydroxyapatite: Hexagonal or Monoclinic? Cryst. Growth Des. 9 (2009) 2991–2994, https://doi.org/10.1021/cg900156w.

[23] Q. Liu, S. Huang, J.P. Matinlinna, Z. Chen, H. Pan, Insight into biological apatite: Physiochemical properties and preparation approaches, Biomed Res. Int. 2013 (2013), https://doi.org/10.1155/2013/929748.

[24] J.A. Lett, K. Ravichandran, M. Sundareswari, The study on the synthetic methodologies for manoeuvring the morphology crystallinity and particle size of hydroxyapatite, J. Chem. Pharm. Res. 7 (2015) 231–239.

[25] T.G. Aguirre, C.L. Cramer, V.P. Torres, T.J. Hammann, T.B. Holland, K. Ma, Effects of the addition of boron nitride nanoplate on the fracture toughness, flexural strength, and Weibull Distribution of hydroxyapatite composites prepared by spark plasma sintering, J. Mech. Behav. Biomed. Mater. 93 (2019) 105–117, https://doi.org/10.1016/j.jmbbm.2019.01.021.

[26] R. Halouani, D. Bernache-Assolant, E. Champion, A. Ababou, Microstructure and related mechanical properties of hot pressed hydroxyapatite ceramics, J. Mater. Sci. Mater. Med. 5 (1994) 563–568, https://doi.org/10.1007/BF00124890.

[27] B. Liu, L. Chen, C. Shao, F. Zhang, K. Zhou, J. Cao, D. Zhang, Improved osteoblasts growth on osteomimetic hydroxyapatite/BaTiO3 composites with aligned lamellar porous structure, Mater. Sci. Eng. C. 61 (2016) 8–14, https://doi. org/10.1016/j.msec.2015.12.009.

[28] Jung, W.K.; Koo, H.C.; Kim, K.W.; Shin, S.; Kim, S.H.; Park, Y.H. Antibacterial Activity and Mechanism of Action of the Silver Ion in Staphylococcus aureus and Escherichia coli. Appl. Environ. Microbiol. **2008**, 74, 2171–2178.

[29] Sütterlin, S.; Tano, E.; Bergsten, A.; Tallberg, A.-B.; Melhus, A. Effects of silver-based wound dressings on the bacterial flora in chronic leg ulcers and its susceptibility in vitro to silver. Acta Derm. Venereol. **2012**, 92, 34–39.

[30] Randall, C.P.; Gupta, A.; Jackson, N.; Busse, D.; O'Neill, A.J. Silver resistance in Gram-negative bacteria: A dissection of endogenous and exogenous mechanisms. J. Antimicrob. Chemother. **2015**, 70, 1037–1046.

[31] Yamanaka, M.; Hara, K.; Kudo, J. Bactericidal Actions of a Silver Ion Solution on Escherichia coli, Studied by Energy-Filtering Transmission Electron Microscopy and Proteomic Analysis. Appl. Environ. Microbiol. **2005**, 71, 7589–7593.

[32] Dakal, T.C.; Kumar, A.; Majumdar, R.S.; Yadav, V. Mechanistic Basis of Antimicrobial Actions of Silver Nanoparticles. Front. Microbiol. **2016**, 7.

[33] Pal, S.; Tak, Y.K.; Song, J.M. Does the antibacterial activity of silver nanoparticles depend on the shape of the nanoparticle? A study of the Gram-negative bacterium Escherichia coli. Appl. Environ. Microbiol. **2007**, 73, 1712–1720.

[34] Kędziora A, Speruda M, Krzyżewska E, Rybka J, Łukowiak A, Bugla-Płoskońska G. Similarities and Differences between Silver Ions and Silver in Nanoforms as Antibacterial Agents. Int J Mol Sci. 2018 Feb 2;19(2):444. doi: 10.3390/ijms19020444. PMID: 29393866; PMCID: PMC5855666.

[35] S. Jafarirad, M. Mehrabi, B. Divband, M. Kosari-Nasab, Biofabrication of zinc oxide nanoparticles using fruit extract of Rosa canina and their toxic potential against bacteria: a mechanistic approach, Mater. Sci. Eng. C 59 (2016) 296–302, https://doi.org/10.1016/j.msec.2015.09.089.

[36] K. Hantke, Bacterial zinc uptake and regulators, Curr. Opin. Microbiol. 8 (2005) 196–202, https://doi.org/10.1016/j.mib.2005.02.001.

[37] B.L. Nairn, Z.R. Lonergan, J. Wang, J.J. Braymer, Y. Zhang, M.W. Calcutt, J. P. Lisher, B.A. Gilston, W.J. Chazin, V. De Cr´ecy-Lagard, D.P. Giedroc, E.P. Skaar, The response of acinetobacter baumannii to zinc starvation, Cell Host Microbe 19 (2016) 826–836, https://doi.org/10.1016/j.chom.2016.05.007.

[38] D.K. Blencowe, A.P. Morby, Zn(II) metabolism in prokaryotes, FEMS Microbiol. Rev. 27 (2003) 291–311, https://doi.org/10.1016/S0168-6445(03)00041-X.

[39] H. Yang, C. Liu, D. Yang, H. Zhang, Z. Xi, Comparative study of cytotoxicity, oxidative stress and genotoxicity induced by four typical nanomaterials: the role of particle size, shape and composition, J. Appl. Toxicol. 29 (2009) 69–78, https://doi.org/10.1002/jat.1385.

[40] K.R. Raghupathi, R.T. Koodali, A.C. Manna, Size-dependent bacterial growth inhibition and mechanism of antibacterial activity of zinc oxide nanoparticles, Langmuir 27 (2011) 4020–4028, https://doi.org/10.1021/la104825u.

[41] U. Kadiyala, E.S. Turali-Emre, J.H. Bahng, N.A. Kotov, J. Scott Vanepps, Unexpected insights into antibacterial activity of zinc oxide nanoparticles against methicillin resistant: Staphylococcus aureus (MRSA), Nanoscale 10 (2018) 4927–4939, https://doi.org/10.1039/c7nr08499d.

[42] R. Pati, R.K. Mehta, S. Mohanty, A. Padhi, M. Sengupta, B. Vaseeharan, C. Goswami, A. Sonawane, Topical application of zinc oxide nanoparticles reduces bacterial skin infection in mice and exhibits antibacterial activity by inducing oxidative stress response and cell membrane disintegration in macrophages, Nanomed. Nanotechnol. Biol. Med. 10 (2014) 1195–1208, https:// doi.org/10.1016/j.nano.2014.02.012.

[43] P.K. Mishra, H. Mishra, A. Ekielski, S. Talegaonkar, B. Vaidya, Zinc oxide nanoparticles: a promising nanomaterial for biomedical applications, Drug Discov. Today 22 (2017) 1825–1834, https://doi.org/10.1016/j. drudis.2017.08.006.

[44] N. Padmavathy, R. Vijayaraghavan, Enhanced bioactivity of ZnO nanoparticles - an antimicrobial study, Sci. Technol. Adv. Mater. 9 (2008), 035004, https://doi. org/10.1088/1468-6996/9/3/035004.

[45] P.V. Pimpliskar, S.C. Motekar, G.G. Umarji, W. Lee, S.S. Arbuj, Synthesis of silver-loaded ZnO nanorods and their enhanced photocatalytic activity and photoconductivity study, Photochem. Photobiol. Sci. 18 (2019) 1503–1511, https://doi.org/10.1039/c9pp00099b.

[46] U. Kadiyala, E.S. Turali-Emre, J.H. Bahng, N.A. Kotov, J. Scott Vanepps, Unexpected insights into antibacterial activity of zinc oxide nanoparticles against methicillin resistant: Staphylococcus aureus (MRSA), Nanoscale 10 (2018) 4927–4939, https://doi.org/10.1039/c7nr08499d.

[47] Maria Godoy-Gallardo, Ulrich Eckhard, Luis M. Delgado, Yolanda J.D. de Roo Puente, Mireia Hoyos-Nogués, F. Javier Gil, Roman A. Perez, Antibacterial approaches in tissue engineering using metal ions and nanoparticles: From mechanisms to applications, Bioactive Materials, Volume 6, Issue 12, 2021, Pages 4470-4490, ISSN 2452-199X, https://doi.org/10.1016/j.bioactmat.2021.04.033.

[48] R.A.A. Festa, D.J.J. Thiele, Copper: an essential metal in biology, Curr. Biol. 21 (2011) R877–R883, https://doi.org/10.1016/j.cub.2011.09.040.

[49] C. Ari¨oz, P. Wittung-Stafshede, Folding of copper proteins: role of the metal? Q. Rev. Biophys. 51 (2018) e4, https://doi.org/10.1017/S0033583518000021.

[50] Y. Wu, W. Wu, W. Zhao, X. Lan, Revealing the antibacterial mechanism of copper surfaces with controllable microstructures, Surf. Coating. Technol. 395 (2020) 125911, https://doi.org/10.1016/j.surfcoat.2020.125911.

[51] M. Vincent, R.E. Duval, P. Hartemann, M. Engels-Deutsch, Contact killing and antimicrobial properties of copper, J. Appl. Microbiol. 124 (2018) 1032–1046, https://doi.org/10.1111/jam.13681.

[52] K. Giannousi, A. Pantazaki, C. Dendrinou-Samara, Copper-based nanoparticles as antimicrobials, in: Nanostructures Antimicrob. Ther. Nanostructures Ther. Med. Ser., Elsevier, 2017, pp. 515–529, https://doi.org/10.1016/B978-0-323-46152- 8.00023-8.

[53] H.K. Abicht, Y. Gonskikh, S.D. Gerber, M. Solioz, Non-enzymic copper reduction by menaquinone enhances copper toxicity in Lactococcus lactis IL1403, Microbiol. 159 (2013) 1190–1197, https://doi.org/10.1099/mic.0.066928-0.

[54] X. Cong, M.F. Poyton, A.J. Baxter, S. Pullanchery, P.S. Cremer, Unquenchable surface potential dramatically enhances Cu2+ binding to phosphatidylserine lipids, J. Am. Chem. Soc. 137 (2015) 7785–7792, https://doi.org/10.1021/ jacs.5b03313.

[55] A.G. Dalecki, C.L. Crawford, F. Wolschendorf, Copper and antibiotics: discovery, modes of action, and opportunities for medicinal applications, in: Adv. Microb. Physiol., Academic Press, 2017, pp. 193–260, https://doi.org/10.1016/bs. ampbs.2017.01.007.

[56] M.D.L. Johnson, T.E. Kehl-Fie, J.W. Rosch, Copper intoxication inhibits aerobic nucleotide synthesis in Streptococcus pneumoniae, Metall 7 (2015) 786–794, https://doi.org/10.1039/c5mt00011d.

[57] A. Hiniker, J.F. Collet, J.C.A. Bardwell, Copper stress causes an in vivo requirement for the Escherichia coli disulfide isomerase DsbC, J. Biol. Chem. 280 (2005) 33785–33791, https://doi.org/10.1074/jbc.M505742200.

[58] A.W. Foster, D. Osman, N.J. Robinson, Metal preferences and metallation, J. Biol. Chem. 289 (2014) 28095–28103, https://doi.org/10.1074/jbc.R114.588145.

[59] L. Macomber, J.A. Imlay, The iron-sulfur clusters of dehydratases are primary intracellular targets of copper toxicity, Proc. Natl. Acad. Sci. U.S.A. 106 (2009) 8344–8349, https://doi.org/10.1073/pnas.0812808106.

[60] V.D. Paul, R. Lill, Biogenesis of cytosolic and nuclear iron-sulfur proteins and their role in genome stability, Biochim. Biophys. Acta Mol. Cell Res. 1853 (2015) 1528–1539, https://doi.org/10.1016/j.bbamcr.2014.12.018.

[61] R.A. Festa, M.B. Jones, S. Butler-Wu, D. Sinsimer, R. Gerads, W.R. Bishai, S. N. Peterson, K.H. Darwin, A novel copper-responsive regulon in Mycobacterium tuberculosis, Mol. Microbiol. 79 (2011) 133–148, https://doi.org/10.1111/ j.1365-2958.2010.07431.x.

[62] A. Ananth, S. Dharaneedharan, M.S. Heo, Y.S. Mok, Copper oxide nanomaterials: synthesis, characterization and structure-specific antibacterial performance, Chem. Eng. J. 262 (2015) 179–188, https://doi.org/10.1016/j.cej.2014.09.083.

[63] Dalecki AG, Crawford CL, Wolschendorf F. Copper and Antibiotics: Discovery, Modes of Action, and Opportunities for Medicinal Applications. *Adv Microb Physiol*. 2017;70:193-260. doi:10.1016/bs.ampbs.2017.01.007.

[64] Bigi A, Foresti E, Gandolfi M, Gazzano M, Roveri N (1995) Inhibiting effect of zinc on hydroxylapatite crystallization. J Inorg Biochem 58:49–58.

[65] M. Shirkhanzadeh, M. Azadegan, G.Q. Liu, Mater. Lett. 24 (1995) 7–12.